ISTANBUL TECHNICAL UNIVERSITY ★ GRADUATE SCHOOL OF SCIENCE ENGINEERING AND TECHNOLOGY

THE DYNAMIC ANALYSIS OF NON-CYLINDRICAL VISCOELASTIC HELICAL BARS USING MIXED FINITE ELEMENT METHOD

M.Sc. THESIS

Merve ERMİŞ

Department of Civil Engineering

Structure Engineering Programme

Thesis Advisor: Prof. Dr. Mehmet H. OMURTAG

MAY 2015

ISTANBUL TECHNICAL UNIVERSITY ★ GRADUATE SCHOOL OF SCIENCE ENGINEERING AND TECHNOLOGY

THE DYNAMIC ANALYSIS OF NON-CYLINDRICAL VISCOELASTIC HELICAL BARS USING MIXED FINITE ELEMENT METHOD

M.Sc. THESIS

Merve ERMİŞ
(501121036)

Department of Civil Engineering

Structure Engineering Programme

Thesis Advisor: Prof. Dr. Mehmet H. OMURTAG

26 MAY 2015

İSTANBUL TEKNİK ÜNİVERSİTESİ ★ FEN BİLİMLERİ ENSTİTÜSÜ

SİLİNDİRİK OLMAYAN VİSKOELASTİK HELİSEL ÇUBUKLARIN KARIŞIK SONLU ELEMAN YÖNTEMİ İLE DİNAMİK ANALİZİ

YÜKSEK LİSANS TEZİ

Merve ERMİŞ
(501121036)

İnşaat Mühendisliği Anabilim Dalı

Yapı Mühendisliği Programı

Tez Danışmanı: Prof. Dr. Mehmet H. OMURTAG

26 MAYIS 2015

Merve ERMİŞ, a **M.Sc.** student of ITU **Graduate School of Science Engineering and Technology** student ID **501121036**, successfully defended the **thesis** entitled "**THE DYNAMIC ANALYSIS OF NON-CYLINDRICAL VISCOELASTIC HELICAL BARS USING MIXED FINITE ELEMENT METHOD**", which she prepared after fulfilling the requirements specified in the associated legislations, before the jury whose signatures are below.

Thesis Advisor :	**Prof. Dr. Mehmet H. OMURTAG** Istanbul Technical University	.....
Jury Members :	**Prof. Dr. Ünal ALDEMİR** Istanbul Technical University	.....
	Prof. Dr. Turgut KOCATÜRK Yıldız Technical University	.....

Date of Submission : 04 May 2015
Date of Defense : 26 May 2015

FOREWORD

This thesis was written for my M.Sc. degree in Structure Engineering Programme of Civil Engineering Department at the İstanbul Technical University. My M.Sc. thesis has made a interesting and informative contribution to me. First, I would like to thank and show my appreciation and gratitude to my thesis advisor Prof. Dr. Mehmet H. OMURTAG for his encouragements, precious suggestions, guidance in writing thesis and instructing me how to study effectively. I would like to thank Assoc. Prof. Dr. Nihal ERATLI for her valuable supports, continuous encouragement, vision and help. Next, I would like to thank Assoc. Prof. Dr. Ahmet Hakan ARGEŞO for his valuable contributions on the field of viscoelasticity and Ass. Prof.Dr. Akif KUTLU, Res. Assist. Dr. Murat YILMAZ for their supports.

I would also like to express my sincere gratitude for my family, their precious supporting me and their advice on how to maintain my motivation during the study of my thesis.

Some part of this research is supported by The Scientific and Technological Research Council of Turkey (Project No. 111M308) and fully supported by the Research Foundation of ITU (Project No. 38078). I would like to thank their financial support.

May 2015

Merve ERMİŞ
Civil Engineer

TABLE OF CONTENTS

Page

LIST OF TABLES

Page

LIST OF FIGURES

Page

LIST OF SYMBOLS

aT	:	Modified Durbin Laplace transformation parameter
t	:	Time parameter
f	:	Force, Function
$\overline{(\ldots)}$	:	Transformed
i	:	Complex number
I	:	Convolution integral
H(...)	:	Heaviside unit function
$\mathcal{L}[...]$	:	Laplace transformation operator
P	:	Force
T	:	Time interval of the solution
z	:	Laplace transformation parameter
$\mathcal{L}^{-1}[...]$	:	Inverse Laplace transformation operator
L_k	:	Lanczos factor
ω	:	Natural frequency
η^E, η^G	:	Damping parameter
τ_r^G	:	Retardation time
$R^G(t)$	:	Relaxation function
R_e^G	:	Equilibrium value of relaxation function
R_0^G	:	Instantaneous value of relaxation function
P, Q	:	Differential operators
σ	:	Stress
ε	:	Strain
$\dot{\varepsilon}$	:	Velocity of strain
s_{ij}, e_{ij}	:	Deviatoric portions of stress and strain tensors
E	:	Elasticity modulus
υ	:	Poisson's ratio
G, μ	:	Shear modulus

η	:	Viscosity coefficient
β^G	:	the ratio of the instantaneous value of relaxation function to the equilibrium value of relaxation function
t_{load}	:	Loading time interval
k'	:	Shear correction factor
u	:	Displacement
M	:	Moment
ρ	:	Material density
α	:	Pitch angle
$R(\varphi)$	:	Centerline radius
$p(\varphi)$	:	Step for unit angle
φ	:	Horizontal angle
$\mathbf{t}, \mathbf{n}, \mathbf{b}$	:	Frenet unit vectors
Ω	:	Rotational vector
$\mathbf{T}$	:	Force vector
$\mathbf{M}$	:	Moment vector
$\mathbf{u}$	:	Displacement vector
$\mathbf{I}$	:	Moment of inertia
$\mathbf{q}$	:	Distributed external force vector
$\mathbf{m}$	:	Distributed external moment vector
$\mathbf{C}$	:	Compliance matrix
$\boldsymbol{\kappa}(\chi, \tau)$	:	Curvature vector
$\mathbf{Q}$	:	Potential operator
$\mathbf{X}^T$	:	Element matrix
$\widehat{(...)}$	:	Known values on the boundary
s^e	:	Helix arc length
χ	:	Curvature
τ	:	Torsion
e	:	Element number

THE DYNAMIC ANALYSIS OF NON-CYLINDRICAL VISCOELASTIC HELICAL BARS USING MIXED FINITE ELEMENT METHOD

SUMMARY

In the case of an elastic material behavior, deformed structure recovers its original shape and size after unloading. The elastic behavior is time independent. The strains measured in a of viscous matrial depend on the speed and intensity of the loading. The viscous behavior is time dependent.Viscoelastic materials exhibit both viscous and elastic effects. In fact, due to internal friction, the material shows some viscous behavior. Thus, for more realistic analysis the viscous behavior should be taken into account. In the literature, There are many models for defining viscoelastic behavior, such as Kelvin, Maxwell and standard model. In this study standard model is prephered due to its suitability for structural analysis.

The viscoelastic materials has been used for so long, and they are preffered for specific applications, such as, to support structures, mechanical equipments, vibration isolatars which are used for reducing the external forces *e.g*. associated with an earthquake or impact forces. In the literature, the studies about viscoelastic isolator have significance for increasing the strength of the structures against the earthquake. For this purpose, viscoelastic helical springs are used to absorb the energy, transfer the forces or reduce the vibration. Helical springs have varios geometries. These may be cylindrical or non-cylindrical, e.g., conical, barrel and hyperboloidal springs. Especially, viscoelastic helices take important place in defence industry.

In this thesis, based on Timoshenko beam theory the dynamic analysis of non-cylindrical viscoelastic helices is investigated. Viscoelastic behavior is modelled by using standard model. By applying the Laplace transformation to the functional, it is carried to the frequency domain. Using the correspondence principle, the constitutive equations of the linear viscoelastic material is identified in the frequency domain. Afterward, applying the variational method to the Laplace transformed functional a mixed finite element is generated. Geometrical properties of conical, barrel and hyperboloidal helical rods are calculated based on the exact expressions, *e.g*., differential arc length and curvatures are determined directly by using the respective axis function of the helical bar. The numerical results obtained after the finite element solution are transformed back to time space by the numerical solution of the modified Durbin's algorithm.

This thesis is composed of six chapters. Chapter 1 is about literaure survey. In Chapter 2, a brief explanation about the Laplace transformation and the inverse Laplace transformation algorithm of modified Durbin's algorithm is given. In Chapter 3, the mechanical viscoelatic model, namely the Standard model, and the application of the correspondance principle is explained. In Chapter 4, the

noncylindrical helical bar geometry is defined by means of the exact expressions, the functional in Laplace space is derived, the finite element formulation is given. The numerical investigation is presented in Chapter 5. A new mixed finite element approach, based on precise definition of the non-cylindrical helical geometry, is verified with the examples existing elastic problems in the literature. Afterward, a convergenge analysis is performed on a viscoelastic hyperbolic helix and finally some viscoelastic benchmark examples are solved. Through the analysis, the time dependent behavior of the cantilever hyperboloidal helix is investigated for some of the viscoelastic parameters, namely, three different values of retardation time of relaxation function associated with the shear modulus, three different values of the ratio of instantaneous value of relaxation function associated with the shear modulus. Also viscoelastic behaviour of three different cross-sectional areas, all having the same net area, namely, a solid circular section, hollow circular section and a thin-walled hollow circular section are investigated. All the results are either tabulated or given as graphics. Discussion of the results are given in Chapter 6.

SİLİNDİRİK OLMAYAN VİSKOELASTİK HELİSELÇUBUKLARIN KARIŞIK SONLU ELEMAN YÖNTEMİ İLE ANALİZİ

ÖZET

Elastik davranış, cisme uygulanan dış kuvvet kaldırıldığında cismin ilk konumuna geri döndüğü durumdur ve bu davranış zamandan bağımsızdır. Viskoz davranış ise cisme uygulanan dış yükler altında meydana gelen şekil değiştirme miktarının yüklemenin hızına ve şiddetine bağlı olduğu durum olup, içinde zaman parametresi içerir. Viskoelastisite ise, yukarıdaki iki tanımın bir karışımı olup, malzemenin hem elastik hem de viskoz etkileri bir arada bulundurduğu davranışı temsil etmektedir. Gerçekte birçok malzeme iç sürtünmelerden dolayı hem elastik hem de viskoelastik davranış sergilemektedir. Burada önemli olan, malzemenin hangi oranlarda bu davranışları yansıttıklarıdır. O nedenle malzeme modellenmesinde viskoelastik davranışın kulanılması daha gerçekçi bir yaklaşım sağlamaktadır. Bu noktada, araştırmacılar farklı mekanik modeller geliştirerek malzeme davranışını formüle etmeye çalışılmaktadır.

Viskoelastik malzemelerin mühendislik uygulamalarındaki yeri geçmişe dayansa da daha çok özgün uygulamalarda karşımıza çıkmaktadır. Son yıllarda gelişen teknoloji ile beraber, örneğin, yapıya gelen deprem etkisini azaltmak amacıyla yapıya kurulan sistemler üzerinde deprem enerjisinin sönümlenmesini sağlayacak mekanik sönümleyiciler ve izolatörler kullanılmaktadır. Literatürde deprem dayanımının artırılması için kullanılan viskoelastik sönümleyiciler üzerine son yıllarda yoğun çalışmaların yapıldığı hepimizin malumudur.

Viskoelastik yaylar, sisteme gelen enerjiyi yutmak, kuvvet aktarımı yapmak, titreşimi sönümlendirerek azaltmak gibi özelliklere sahip dönel simetrik yapı elemanlarıdır. Silindirik olmayan helislere örnek olarak konik, fıçı ve hiperboloidal türü helisel çubuklar verilebilir. Ayrıca, viskoelastik özelliği olan helisler özellikle savunma sanayinde de önemli bir yer bulmaktadır.

Viskoelastik malzemeye ait zamana bağlı davranışı ifade edebilmek için bünye bağıntılarında zaman değişkeni de göz önüne alınmaktadır. Bu amaçla, malzemede zamana bağlı davranışı inceleyebilmek için bir viskoelastik gerilme analizi yöntemine ihtiyaç vardır. Bu konuda, bünye bağıntılarının zamana göre davranışını tariflerken basit çözümler sunan ve matematiksel bir tanım veren doğrusal viskoelastisite kuramından yararlanılır. Doğrusal viskoelastik malzemelerde toplam gerilme elastik gerileme ve sönümleyici gerilme bileşenlerinin toplamından oluşmaktadır. Basit mekanik modellerle tanımlanan viskoelastik malzeme davranışında, yaylar elastik davranışı, sönümleyiciler ise viskoz davranışı tanımlamakta kullanılır. Standard model ise toplamda iki yay ve bir sönüm kutusundan oluşan bir mekanik modeldir. Bu elemanlardan, yay ve sönümleyicinin birbirlerine paralel bağlanarak, bu paralel bağlı yapının da diğer yay ile seri bağlanmasıyla standart model ifade edilir. Standart modele ait viskoelastik model davranışı eksenel yük durumu ilişkilendirilerek verilmiştir. Gerilme-şekil değiştirme

ilişkisi modele ait gevşeme fonksiyonu üzerinden tanımlanmıştır. Literatürde, viskoelatik davranışı tarifleyen, Kelvin, Maxwell, standart model gibi birçok model bulunmaktadır. Bunlar arasında katı cisimler mekaniğine en uygun olanları Kelvin ve Standart model olup, Maxwell akışkanlar için daha uygundur.

Viskoelatik problemler genel anlamda zaman uzayında çözülürler. Öte yandan, doğrusal viskoelastik problemler frekans uzayında da incelenebilir. Bu amaçla Fourier ya da Laplace uzaylarına geçilir, hesaplar tamamlandıktan sonra sonuçlar geri dönüşüm yöntemleri ile zaman uzayına aktarılır. Frekans uzayı çözümlerinde Laplace çözümleri çok daha fazla tercih edilmektedir. Laplace dönüşümü, integral dönüşümleri olarak da adlandırılır ve lineer viskoelastik sistemlerin analizinde kullanılan bir yöntemdir. Laplace dönüşümü ile zaman uzayında çözümü zor olan bir problem frekans uzayında çözümü daha kolay olan bir probleme dönüşür. Çubuğa ait fonksiyonel frekans uzayına taşınırken, Laplace dönüşümü zamana bağlı olan türev ve integralleri, dönüşüm parametresi cinsinden matematiksel ifadelere dönüştürür. Aynı zamanda, viskoelastik malzemeyi tanımlayan parametreler ise karşıgelim ilkesi kullanılarak frekans uzayındaki kompleks karşıtları ile yer değiştirir. Karşıgelim ilkesi, elastik cisme ait bünye bağıntılarına karşı gelen, viskoelastik bünye bağıntılarının bulunmasını sağlayan matematiksel bir analoji yöntemidir. Böylece viskoelastik problem, karşıgelim ilkesi kullanılarak çözümü Laplace uzayında gerçekleştirilen bir çeşit elastik probleme dönüştürülür. Daha sonra sonuçlara uygulanan ters dönüşümler ile zaman uzayına geçilir.

Bu tez kapsamında eksen geometrisi silindirik olmayan viskoelastik helislerin dinamik analizi Timoshenko çubuk kuramı üstünden yapılmıştır. Timoshenko çubuk kuramı çerçevesinde dönel eylemsizlikleri de hesaba katılmıştır. Özellikle dinamik problemler açısından bu nokta önem arz etmektedir. Bu çalışma kapsamında, malzemenin viskoelastik davranışı standart model üzerinden tariflendi, çözümler Laplace uzayında gerçekleştirildi ve bu çerçevede kesiti dolu, ince ve kalın cidarlı halka olan ve çubuk eksen geometrisi silindirik olmayan helisler incelendi.

Standart model için elastik-viskoelastik analoji işlem adımlarından bahsedecek olursak; standart modele ait, tek boyutlu doğrusal viskoelastik gerilme- şekil değiştirme bağıntısı deviyatorik bileşenler cinsinden ifade edilerek viskoelastik malzemeye ait denge denklemi elde edildi. Bu çalışma kapsamında Laplace uzayında dönüşüm parametreleri üzeri çizgili sembol ile gösterilmiştir. Öncelikle denge denklemi Laplace uzayına taşınır ve karşıgelim ilkesinden yararlanılarak malzeme sabitleri frekans uzayındaki kompleks karşıtları cinsinden elde edilir. Standart modele ait kompleks kayma modülü bazı parametrelere bağlıdır. Bu parametrelerden biri olan gecikme zamanı, kayma modülü ve sünme fonksiyonu ile ilişkili bir büyüklüktür. Aynı zamanda, sünme fonksiyonunun denge konumu olan kayma modülüne yaklaşma hızının bir ölçütüdür. Diğer bir parametre ise sünme fonksiyonunun başlangıç değerinin yine sünme fonksiyonunun denge değerine oranıdır.

Bu çalışmada, Timoshenko çubuk kuramına bağlı silindirik olmayan viskoelastik çubukların dinamik analizi yapıldı. Viskoelastik davravranış standart model üzerinden tanımlandı.Frekans uzayına aktarılmış fonksiyonel üstünden varyasyonel işlemlerle sonlu eleman formülasyonuna geçilirken, bu çalışmaya özgü olan konik, fiçı ve hiperboloidal türü helislerin geometrik özelliklerini tarifleyen diferansiyel yay uzunluğu, eğrilik fonksiyonları işlemlere kesin değerleri ile katılmıştır. Frekans

uzayında elde edilen sonlu eleman sonuçlarının zaman uzayındaki değerleri ters Laplace dönüşümü (modifiye Durbin algoritması) kullanılarak elde edilmiştir.

Bu tez altı bölümden meydana gelmektedir. Birinci Bölüm , literatür araştırması ile ilgili kısımdır. İkinci bölüm, Laplace dönüşümü ve modifiye Durbin ters Laplace dönüşümü ile ilgili özet açıklamayı içermektedir. Üçüncü bölümde, viskoelastik malzeme olarak standart model ele alınarak ve karşıgelim ilkesine ait uygulamanın nasıl olacağı açıklanmıştır. Dördüncü bölümde, silindirik olmayan helisel çubuk geometrisi helise ait tam ifadeler üzerinden tariflenip, Laplace uzayındaki fonksiyonel elde edilip, sonlu eleman formülasyonu verilmiştir. Nümerik hesaplamalarla ilgili araştırmalar beşinci bölümde verilmiştir. Bu bölümde, yeni sonlu eleman formülasyonu silindirik olmayan helis geometrisin kesin tanımı üzerinden tanımlanmıştır. Bu formülasyon literatürde bulunan elastik problemler ile doğrulanmıştır. Daha sonra, viskoelastik hiperbol helis için yakınsama analizi yapılarak, orjinal viskoelastik örneklerin çözümüne yer verilmiştir. Analizler boyunca, bir ucundan rijit tutturulmuş diğer ucu serbest hiperbol helisin zamana bağlı davranışı çeşitli parametreler açısından incelenmiştir. Viskoelastik malzemeyi tanımlayan parametreleri tekrar hatırlayacak olursak bu parametrelere göre analiz sırasıyla, kayma modülü ile ilgili gevşeme fonksiyonuna ait gecikme zamanının üç farklı değeri için analizine, ve ayrıca kayma modülü ile ilşkili gevşeme fonksiyonuna ait oranın üç farklı değeri için analize yer verilmiştir. Daha sonra, net alanları birbirlerine eşit üç farklı kesit geometrisine ait viskoelastik davranış ele alınmıştır. Bu kesitler sırasıyla dolu dairesel kesit, kalın ve ince cidarlı dairesel kesitlerdir. Elde edilen sonuçlar tablo ve grafikler şeklinde sunulmuştur. Sonuçlarla ilgili yorumlara ise altıncı bölümde yer verilmiştir.

1. INTRODUCTION

Helical springs recovers its original shape and size completely or partially after unloading. They have significant applications in engineering structures as mechanical devices, which are used to reduce vibration, to absorb shock or to maintain a force between contacting surfaces. In addition, they are utilized as helical carrier systems, particularly as stairs. In literature, most of the helicodal bar studies are based on elastic behavior, and studies about viscoelastic helical springs are limited. In fact, due to the internal friction, viscous behaviors may appear in the material and in such cases the viscous effects of the material should be considered. The theoretical studies about viscoelasticity of Flügge (1975), Christensen (1982) can be given as background studies. Viscoelastic materials that are used in civil engineering structures are made of typical carbon polymers or similar solid materials (Aldemir and Aydın, 2005). Helical springs and viscoelastic dampers are used under machine foundation for the aim of distributing energy (Tezcan and Uluca, 2003).

1.1 Literature Review

The free vibration analysis of non-cylindrical helical springs are investigate by using transfer matrix method (Yıldırım and İnce, 1997; Nagaya *et al*., 1986, Yıldırım, 1997), the stiffness matrix method (Yıldırım, 1998; Yıldırım, 2002; Busool and Eisenberger, 2002), the mixed finite element method (Girgin, 2006) and the pseudospectral method (Lee, 2007). Free vibration analysis of composite helical bars were investigated by Yıldırım (1999, 2001a, 2001b, 2004), Yıldırım *et al*. (1999) and Yıldırım and Sancaktar (2000). Dynamic analysis of viscoelastic, anisotropic spatial curved systems is investigated by Çalım, 2003. Also, forced vibration analysis of isotropic homogeneous or composite helical rods were investigated (Temel and Çalım, 2003; Temel *et al*., 2005; Çalım 2009a, 2009b).

A mathematical analogy called the correspondence principle permits the determination of the viscoelastic stresses and strains in a body from the corresponding elastic stresses and strains in the same body Lee (1955). This

technique is first applied to incompressible materials by Alfrey (1948) and is extended by Tsien (1950) and Read (1950). Findley *et al*. (1976) used correspondence and superposition principles for solving equations of viscoelastic beam. Yamada *et al*. (1974) investigated free vibration of viscoelastic rods. Kıral *et al.* (1976) investigated the naturally curved and twisted linearly viscoelastic Timoshenko rods with square cross-section subjected to arbitrary time depend loading including rotary inertia under the assumption of infinitesimal displacements and their gradients. Chen and Lin (1982) investigated dynamic behaviors of viscoelastic straight beams by Finite element method. White (1968) introduced a stress analysis method based on linear viscoelasticity and hereditary integral form of stress-strain relation. Payette and Reddy (2010) studied nonlinear quasi-static bending and extension of initially straight linearly viscoelastic Euler-Bernoulli and Timoshenko beams with square cross-section. Kocatürk and Şimşek (2004) analyzed the transverse vibration of a Kelvin model viscoelastic Euler-Bernoulli simply supported beam constant cross-section with intermediate point constraints subjected to a moving harmonic load, Kocatürk and Şimşek (2006a) analyzed the problem of lateral vibration of a Kelvin-Voigt model viscoelastic Bernoulli-Euler simply supported beam subjected to an eccentric compressive force and a harmonically varying transverse concentrated moving force and Kocatürk and Şimşek (2006b) analyzed the dynamic response of eccentrically prestressed Kelvin-Voigt model viscoelastic Timoshenko simply supported beams under a moving harmonic load with constant axial speed. Temel (2004), Temel *et al.* (2004), Temel and Çalım (2003), Temel *et al.* (2003) and Çalım and Temel (2002) investigated the quasi-static and dynamic analysis of viscoelastic straight and helical beams in the Laplace domain. By using the complementary functions method, the ordinary differential equations based on Timoshenko beam theory are solved numerically.

Based on the Gáteaux differential and the mixed finite element method, chronological studies are Kadıoğlu (1999), Aköz and Kadıoğlu (1999), Kadıoğlu and Aköz (2003), Cebecigil (2005), Yükseloğlu (2005), Arıbaş (2012) and Eratlı *et al* (2014) but only in the last two studies the rotary inertia is considered which is essential in Timoshenko theory. Dynamic analysis of cylindrical and non-cylindrical viscoelastic helical rods with circular and non-circular sections is dealt by Arıbaş (2012). Dynamic analysis of cylindrical and conical viscoelastic helical rods with

rectangular section is investigated by Eratlı *et al* (2014) and influence of rotary inertia is discussed with details.

1.2 Purpose of the Thesis

In this study, dynamic analysis of non-cylindrical viscoelastic helical rods with solid circular, hollow circular and thin-walled hollow circular cross-sections is investigated. The functional developed by Omurtag and Aköz (1992) for elastic helical rods is suitable for the mixed finite element analysis. Geometry of the non-cylindrical helical rods are determined using the exact geometry expressions, namely the differential arc length and curvatures, hence the corresponding element generations are based on them.

The linear viscoelastic behavior of the material is modeled by using the Standard model. In the Laplace domain, elastic-viscoelastic analogy (correspondence principle) is used and the material parameters are replaced with their complex counterparts in the Laplace space. Mixed finite element solution is done in Laplace domain and then the results are transformed back to time space numerically by modified Durbin's algorithm (Narayanan, 1980) that is developed from Dubner and Abate (1968) and Durbin (1974).

The new proposed formulation is verified by solving the examples of elastic conical, barrel and hyperboloidal helical bars (see Examples 1.1-1.3). A convergence test is carried on the dynamic response of a viscoelastic cantilever hyperboloidal helical bar (see Exampe 3-1). As benchmark examples, the influence of viscous parameters (τ_r^G the retardation time and β^G the ratio associated with shear modulus) (see Examples 3.2 and 3.3), the number of active turns (see Example 3.4) and the section geometry for solid-circular, hollow-circular and thin-walled hollow-circular (see Example 3.5) are investigated.

2. THE LAPLACE TRANSFORMATION METHOD

2.1 The Laplace Transformation

The Laplace transform converts integral and differential equations into algebraic equations from time domain to frequency domain. This transformation method is used for the analysis of linear systems and makes it easier to solve ordinary differential equations. The result in frequency domain can be transformed back to time domain by using inverse Laplace transformation methods. The Laplace transformation of a time dependent function $f(t)$, for $t > 0$,

$$\mathcal{L}[f(t)] := \bar{f}(z) \quad \text{and} \quad \bar{f}(z) := \int_0^\infty f(t)\, e^{-zt} \mathrm{d}t \tag{2.1}$$

where, z is the Laplace transformation parameter (Spiegel 1965). The Laplace transformation of a first-order and a second-order time-dependent derivatives of $f(t)$ are

$$\mathcal{L}[\dot{f}(t)] = z\, \bar{f}(z) - f(0) \tag{2.2}$$

$$\mathcal{L}[\ddot{f}(t)] = z^2\, \bar{f}(z) - z\, f(0) - \dot{f}(0) \tag{2.3}$$

where,

$$\frac{\mathrm{d}f}{\mathrm{d}t} = \dot{f} \quad , \quad \frac{\mathrm{d}^2 f}{\mathrm{d}t^2} = \ddot{f} \tag{2.4}$$

The terms $f(0)$, $\dot{f}(0)$ are the initial conditions of $f(t)$ at $t = 0$. The Laplace transform of some analytical functions can be obtained in closed form (see Table 2.1)

2.2 Durbin's Modified Inverse Laplace Transformation Method

By definition, the inverse Laplace transform is,

$$\mathcal{L}^{-1}[\bar{f}(z)] := f(t) \tag{2.5}$$

$$f(t) := \frac{1}{2\pi i}\int_{a-i\infty}^{a+i\infty} \bar{f}(z)\, e^{zt}\,\mathrm{d}z \tag{2.6}$$

where, is an arbitrary constant bigger than zero that removes singularity in all real parts of $\bar{f}(z)$. In this section Durbin's modified inverse Laplace transformation method, one of the inverse Laplace transformation method. It was developed from Dubner and Abate's method based on finite Fourier-Cosine transformation (Dubner and Abate, 1968). Durbin's numerical inverse Laplace transformation method (Durbin, 1974) is given by

$$f\left(t_j\right) \cong \frac{2e^{aj\Delta t}}{T}\left[-\frac{1}{2}\mathrm{Re}\left\{\bar{f}\left(a\right)\right\} + \mathrm{Re}\left\{\sum_{k=0}^{N-1}\left(A\left(k\right)+iB\left(k\right)\right)e^{i(2\pi/N)jk}\right\}\right] \tag{2.7}$$

$$A(k) = \sum_{I=0}^{L} \mathrm{Re}\left\{\bar{f}\left(a+i\left(k+IN\right)\frac{2\pi}{T}\right)\right\} \tag{2.8}$$

$$B(k) = \sum_{I=0}^{L} \mathrm{Im}\left\{\bar{f}\left(a+i\left(k+IN\right)\frac{2\pi}{T}\right)\right\} \tag{2.9}$$

where, i is the imaginary unit, T is the time period of the solution, N is the equal time periods, $z_k = a+(i2\pi k/T)$ is k^{th} Laplace transformation parameter, $t_j = j\Delta t = jT/N, (j = 0,1,2,....,N-1)$ and,

$$a = \frac{aT}{T}\cdot \tag{2.10}$$

For the time interval $0 \le t \le T$, the function $f(t)$ is calculated. It was indicated that satisfactory precision can be obtained for $5 \le aT \le 10$ in Durbin (1974). In Eqn. **(2.7)**, the second part of the equality between the brackets is

$$\sum_{k=0}^{N-1}\left[A\left(k\right)+iB\left(k\right)\right]e^{i(2\pi/N)jk} \tag{2.11}$$

calculated by using a Fast Fourier Transform sub-program in order to attain a better convergence (Brigham, 1974). Eqn. **(2.7)** can also be modified according to the Narayanan's suggestion (Narayanan, 1979)

$$f(t_j) \cong \frac{2e^{aj\Delta t}}{T}\left[-\frac{1}{2}\mathrm{Re}\left\{\bar{f}\left(a\right)\right\} + \mathrm{Re}\left\{\sum_{k=0}^{N-1}\left\{\bar{f}\left(z_k\right)\mathrm{L}_k\right\}e^{i(2\pi/N)jk}\right\}\right] \tag{2.12}$$

Table 2.1 : Laplace transforms in closed form of some functions defined in time space (Arıbaş 2012).

Load Types	Time space $f(t)$	Laplace Transform $\overline{f}(z)$
Step type	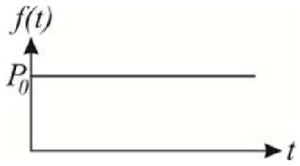	$\frac{P_0}{z}$
Rectangular Impulse	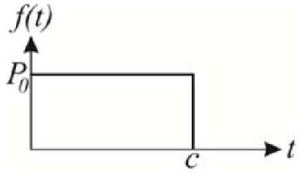	$\frac{P_0\left(1-e^{-cz}\right)}{z}$
Triangle Impulse	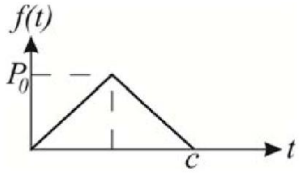	$P_0\left[\frac{1-e^{-\frac{1}{2}cz}}{z}\right]^2\frac{2}{c}$
Right Triangle Impulse	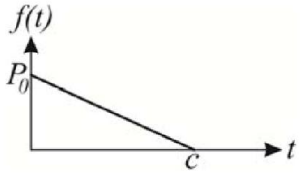	$P_0\left[\frac{1}{z}-\frac{1-e^{-cz}}{cz^2}\right]$
Sinusoidal Impulse	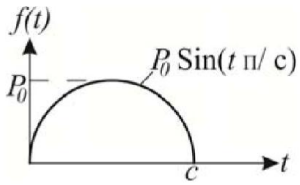	$P_0\frac{\pi c\left(1+e^{-cz}\right)}{c^2z^2+\pi^2}$
Periodical Rectangular	$2\sum_{k=0}^{\infty}(-1)^k\,\mathrm{H}(t-2k)$	$\frac{2}{z\left(1+e^{-2z}\right)}$
Heaviside Unit Function	$\mathrm{H}(t-25)$	$\frac{e^{-25z}}{z}$
Increasing Sinus	$\frac{1}{2}t\sin t$	$\frac{z}{\left(z^2+1\right)^2}$

where, each term of discrete values that is calculated in the Laplace domain is modified by multiplying Lanczos $\left(\mathrm{L}_k\right)$ factor. These factors are given by,

$$\mathrm{L}_k \quad : \quad \begin{cases} =1 & , \quad k=0 \\ =\dfrac{\sin\left(\dfrac{k\pi}{N}\right)}{\dfrac{k\pi}{N}} & , \quad k>0 \end{cases} \qquad \textbf{(2.13)}$$

3. MECHANICAL MODELLING OF VISCOELASTICITY: STANDARD MODEL

3.1 The Constitutive Equations

For a viscoelastic material the total stress σ can be decomposed into two parts as,

$$\sigma = {}_E\sigma + {}_D\sigma \tag{3.1}$$

where, ${}_E\sigma$ and ${}_D\sigma$ account for the elastic and dissipative stress components respectively. The viscoelastic material behavior is simulated using some simple mechanical models (Kelvin model, Standard model, *etc.*). In these models, springs are used to present the contributions of elastic stresses whereas dashpots are used to represent the contributions of dissipative stresses. The constitutive equation of viscoelastic behavior includes time as a variable in addition to stress and strain variables. Also speed of the loading and its duration effects the strains.

The general linear differential one-dimensional viscoelastic stress-strain relation can be written as follows:

$$\mathrm{P}\sigma = \mathrm{Q}\varepsilon \tag{3.2}$$

by neglecting the thermal effect (Boley and Weiner, 1960), where P and Q are the differential operators, and they can be defined as follows:

$$\mathrm{P} = \mathrm{a}_m \frac{\partial^m}{\partial t^m} + \mathrm{a}_{m-1} \frac{\partial^{m-1}}{\partial t^{m-1}} + \cdots + \mathrm{a}_1 \frac{\partial}{\partial t} + \mathrm{a}_0 \tag{3.3}$$

$$\mathrm{Q} = \mathrm{b}_n \frac{\partial^n}{\partial t^n} + \mathrm{b}_{n-1} \frac{\partial^{n-1}}{\partial t^{n-1}} + \cdots + \mathrm{b}_1 \frac{\partial}{\partial t} + \mathrm{b}_0 \tag{3.4}$$

3.2 The Standard Model

In this study, the linear viscoelastic material behavior is considered by using Standard model (see Figure 3.1) and the stress-strain time variations (behaviors) of

the Standard model is discussed through the relaxation function (Findley *et al.* 1976, Arıbaş 2012, Eratlı *et al.* 2014). The stress-strain relation for the Standard model is,

$$\dot{\sigma} + \frac{(E_1 + E_2)}{\eta}\sigma = E_1\,\dot{\varepsilon} + \frac{(E_1\,E_2)}{\eta}\varepsilon \tag{3.5}$$

or

$$\frac{\dot{\sigma}}{E_1} + \frac{(E_1 + E_2)}{E_1\eta}\sigma = \dot{\varepsilon} + \frac{(E_1\,E_2)}{E_1\eta}\varepsilon \tag{3.6}$$

where η is the viscosity coefficient of the dashpot, $\dot{\varepsilon}$ is the velocity of strain and, E_1, E_2 are the elastic parameters. We can rewrite Eqn. **(3.5)** in terms of the deviatoric portions,

$$\frac{1}{2\mu}\dot{s}_{ij} + \frac{1}{2\eta}s_{ij} = \dot{e}_{ij} + \zeta\, e_{ij} \tag{3.7}$$

where $\zeta = \mu/\eta$ (Boley and Weiner, 1960). By comparing Eqn. **(3.7)** with $\mathrm{P}\,s_{ij} = \mathrm{Q}\,e_{ij}$ and we obtain the equilibrium equation $\sigma_{ij,j} = 0$ for the viscoelastic material.

3.3 The Correspondence Principle

A brief explanation of the elastic and the viscoelastic stress-strain relations and the viscoelastic-elastic analogy is as follows. First, the equilibrium equation $\sigma_{ij,j} = 0$ is transformed into Laplace space. By means of the correspondence principle, which is well documented in Boley and Weiner (1960), the transformed material parameters can be obtained quite easily. By means of the correspondence principle, the solution of a linear viscoelastic problem in Laplace domain can be obtained from the corresponding solution of linear elastic problem by replacing the elastic constants with the complex moduli according to the chosen viscoelastic models. Assuming homogenous initial conditions, the Laplace transform of Eqn. **(3.2)** becomes

$$\overline{\mathrm{P}}^{E}\overline{\sigma} = \overline{\mathrm{Q}}^{E}\overline{\varepsilon} \tag{3.8}$$

where, the transformed terms in the Laplace domain are defined by the over bared notation $\overline{(\ldots)}$. Consequently, by means of the correspondence principle, the relations

between elastic material constants and the viscoelastic material constants can be obtained. Thus, the operators $\overline{\mathrm{P}}^E$ and $\overline{\mathrm{Q}}^E$

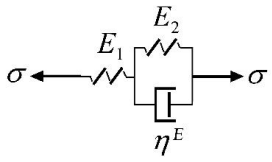

Figure 3.1 : The Standard Model

$$\overline{\mathrm{P}}^E = \left[1 + \frac{\eta^E}{E_1 + E_2} z\right];\ \overline{\mathrm{Q}}^E = \frac{E_1 E_2}{E_1 + E_2}\left[1 + \frac{\eta^E}{E_1 + E_2} z\right] \tag{3.9}$$

If the viscoelastic material exhibits the standard type of distortional behavior then the complex shear modulus can be expressed in the form

$$\overline{G} = G\left[\frac{(1 + \beta^G \tau_r^G z)}{(1 + \tau_r^G z)}\right] \tag{3.10}$$

The detailed information exists in Mengi *et al.* (2006) and Baranoglu *et al.* (2006).

$$G = \frac{G_1 G_2}{G_1 + G_2} \tag{3.11}$$

$$\tau_r^G = \frac{\eta^G}{G_1 + G_2} \tag{3.12}$$

Note that, Eq. **(3.10)** is written in view of the equation given for the standard model in Eq. (3.9), by replacing the elastic and damping parameters E_1, E_2 and η^E with G_1, G_2 and η^G, respectively. τ_r^G is the retardation time of relaxation function associated with shear modulus that is given by $R^G(t) = G\left[1 + (\beta^G - 1)\exp(-t/\tau_r^G)\right]$. From Figure 3.2, it is seen that τ_r^G measures how fast relaxation function approaches to its equilibrium value G. β^G is the ratio of instantaneous value of relaxation function $R_0^G = R(0) = G_1$ to the equilibrium value of relaxation function $R_e^G = \lim_{t\to\infty} R^G(t) = G$, that is,

$$\beta^G = \frac{R_0^G}{R_e^G} = \frac{G_1 + G_2}{G_2} > 1 \tag{3.13}$$

and is non-dimensional by definition.

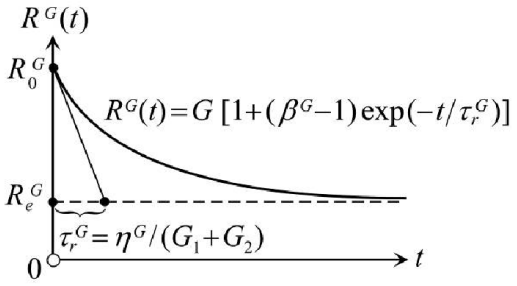

Figure 3.2 : Relaxation function of the standard model associated with shear modulus.

The solution of a linear viscoelastic problem in the Laplace domain is obtained from the corresponding solution of linear elastic problem by replacing the elastic constants with the complex moduli according to the selected viscoelastic model (Shames and Cozarelli 1997).

4. FUNCTIONAL AND FINITE ELEMENT MODELLING FOR NON-CYLINDRICAL HELICAL BARS

In this part, the helix geometry, the field equations, functional and finite element formulation are discussed for the non-cylindrical helicodal bars (Fig. 4.1) in detail.

4.1 The Non-Cylindrical Helix Geometry

The geometrical properties of the helix in the Cartesian coordinate system in Fig. 4.1 are

$$x = R(\varphi)\cos\varphi, \quad y = R(\varphi)\sin\varphi, \quad z = p(\varphi)\varphi, \quad p(\varphi) = R(\varphi)\tan\alpha \qquad \textbf{(4.1)}$$

where α denotes the pitch angle, $R(\varphi)$ and $p(\varphi)$ signify the centerline radius and the step for unit angle of the helix as a function of the horizontal angle φ respectively. The horizontal radius of any point on the centroidal axis of helix is defined by using the following formulae:

Barrel and hyperboloidal helix:

$$R(\varphi) = R_1 + (R_2 - R_1)\left(1 - \frac{\varphi}{n\pi}\right)^2 \qquad \textbf{(4.2)}$$

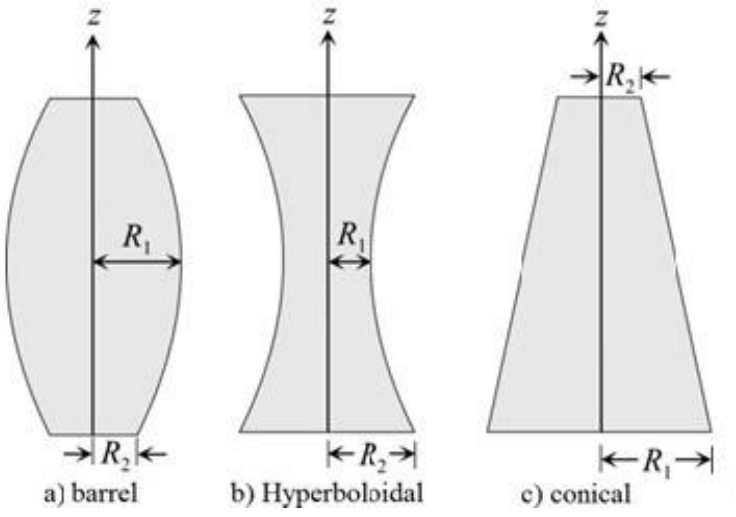

Figure 4.1 : The non-cylindrical helical geometries.

Conical Helix:

$$R(\varphi) = R_1 + \frac{(R_2 - R_1)\varphi}{2n\pi} \tag{4.3}$$

where φ is the horizontal angle, n is the number of active turns of helix, respectively. Curvatures of the non-cylindrical helical bars are derived based on the fundamental equations of a cylindrical helix $c = \sqrt{R^2 + p^2}$ and $\mathrm{d}s = c\,\mathrm{d}\varphi$. In accordance with this assumption, the equations of the non-cylindrical helical geometries are derived. The infinitesimal arc length $\mathrm{d}s$ in Frenet coordinate system,

$$\mathrm{d}s = \sqrt{R^2(\varphi) + p^2(\varphi)}\,\mathrm{d}\varphi = c(\varphi)\,\mathrm{d}\varphi \tag{4.4}$$

the curvature and torsion of the helix axis are given in Eqns. (4.4) and (4.5)

$$\frac{\mathrm{d}\mathbf{t}}{\mathrm{d}s} = \chi\,\mathbf{n}, \quad \frac{\mathrm{d}\mathbf{n}}{\mathrm{d}s} = -\chi\,\mathbf{t} + \tau\,\mathbf{b}, \quad \frac{\mathrm{d}\mathbf{b}}{\mathrm{d}s} = -\tau\,\mathbf{n} \tag{4.5}$$

The unit vectors of Frenet coordinate system are $\mathbf{t}, \mathbf{n}, \mathbf{b}$ where $\mathbf{t}$ is the tangential vector to the helix centerline, $\mathbf{n}$ is the unit normal vector and $\mathbf{b} = \mathbf{t} \times \mathbf{n}$ is the binormal vector.

$$\begin{aligned} c(\varphi) &= \sqrt{R^2(\varphi) + p^2(\varphi)} \\ \chi &= \frac{R(\varphi)}{c^2(\varphi)} \\ \tau &= \frac{p(\varphi)}{c^2(\varphi)} \\ p(\varphi) &= R(\varphi)\tan\alpha \end{aligned} \tag{4.6}$$

4.2 The Field Equations of Elastic Helix

The field equations based on elastic Timoshenko beam theory for a helical bar are (Olgun, 2004),

Equation of motion

$$-\frac{\mathrm{d}\mathbf{T}}{\mathrm{d}s} - \mathbf{q} + \rho A\,\ddot{\mathbf{u}} = \mathbf{0} \tag{4.7}$$

$$-\frac{\mathrm{d}\mathbf{M}}{\mathrm{d}s} - \mathbf{t} \times \mathbf{T} - \mathbf{m} + \rho \mathbf{I}\,\ddot{\boldsymbol{\Omega}} = \mathbf{0} \tag{4.8}$$

Kinematic equations

$$\frac{\mathrm{d}\mathbf{u}}{\mathrm{d}s}+\mathbf{t}\times\boldsymbol{\Omega}-\boldsymbol{\gamma}=\mathbf{0} \tag{4.9}$$

$$\frac{\mathrm{d}\boldsymbol{\Omega}}{\mathrm{d}s}-\boldsymbol{\kappa}=\mathbf{0} \tag{4.10}$$

Constitutive equations

$$\boldsymbol{\gamma}-\mathbf{C}_{\gamma}\mathbf{T}=\mathbf{0} \tag{4.11}$$

$$\boldsymbol{\kappa}-\mathbf{C}_{\kappa}\mathbf{M}=\mathbf{0} \tag{4.12}$$

where, in Frenet form,

the displacement vector : $\mathbf{u}=u_t\,\mathbf{t}+u_n\,\mathbf{n}+u_b\mathbf{b}$,

the cross-section rotation vector : $\boldsymbol{\Omega}=\Omega_t\,\mathbf{t}+\Omega_n\,\mathbf{n}+\Omega_b\mathbf{b}$,

the force vector : $\mathbf{T}=T_t\,\mathbf{t}+T_n\,\mathbf{n}+T_b\mathbf{b}$ and

the moment vector : $\mathbf{M}=M_t\,\mathbf{t}+M_n\,\mathbf{n}+M_b\mathbf{b}$.

Also, ρ is the density of material, A is area of the cross-section, $\mathbf{I}$ is the moment of inertia. $\mathbf{q}$ and $\mathbf{m}$ are the distributed external force and moment vectors. $\mathbf{C}_{\kappa}$ and $\mathbf{C}_{\gamma}$ are compliance matrices for elastic material Omurtag and Aköz (1992).

4.3 The Field Equations in The Frequency Domain

To solve viscoelastic helix problems, the field equations which are mentioned in Eqns. **(4.7) - (4.12)** must be defined in the frequency domain. For the sake of the simplicity, let us write them in the Laplace space. Therefore, by using the definition in Eqns. **(2.2)** and **(2.3)** , the field equations in the Laplace space are obtained as follows:

Equation of motion;

$$-\frac{\mathrm{d}\overline{\mathbf{T}}}{\mathrm{d}s}-\overline{\mathbf{q}}+\rho A z^2\,\overline{\mathbf{u}}=\mathbf{0} \tag{4.13}$$

$$-\frac{\mathrm{d}\overline{\mathbf{M}}}{\mathrm{d}s}-\mathbf{t}\times\overline{\mathbf{T}}-\overline{\mathbf{m}}+\rho\mathbf{I}z^2\;\overline{\boldsymbol{\Omega}}=\mathbf{0} \tag{4.14}$$

Kinematic equations;

$$\frac{\mathrm{d}\bar{\mathbf{u}}}{\mathrm{d}s}+\mathbf{t}\times\bar{\boldsymbol{\Omega}}-\bar{\boldsymbol{\gamma}}=\mathbf{0} \tag{4.15}$$

$$\frac{\mathrm{d}\bar{\boldsymbol{\Omega}}}{\mathrm{d}s}-\bar{\boldsymbol{\kappa}}=\mathbf{0} \tag{4.16}$$

Constitutive equations;

$$\bar{\boldsymbol{\gamma}}-\bar{\mathbf{C}}_{\gamma}\bar{\mathbf{T}}=\mathbf{0} \tag{4.17}$$

$$\bar{\boldsymbol{\kappa}}-\bar{\mathbf{C}}_{\kappa}\bar{\mathbf{M}}=\mathbf{0} \tag{4.18}$$

where z is the Laplace transformation parameter and the quantities ($\bar{\mathbf{u}},\cdots,\bar{\mathbf{M}}$, *etc.*) which are defined by the over bared notation in the Eqns. **(4.13) - (4.18)** show the equivalent in the Laplace domain. For Eqns. **(4.17)** and **(4.18)** see Arıbaş (2012) and Eratlı *et al*. (2014).

4.4 The Functional in The Frequency Domain

The field equations which are given in Eqns. **(4.13) - (4.18)** can be written in operator form $\bar{\mathbf{Q}}=\bar{\mathbf{L}}\bar{\mathbf{y}}-\bar{\mathbf{f}}$ and the matrix form of the operator is given as follows:

$$\mathbf{Q}=\left[\begin{array}{cccccc|cccc}
\rho A z^2 & 0 & 0 & -(\cdots)_{,s} & 0 & 0 & 0 & 0 & 0 & 0\\
0 & \rho\mathbf{I} z^2 & -(\cdots)_{,s} & -\mathbf{t}\times & 0 & 0 & 0 & 0 & 0 & 0\\
0 & (\cdots)_{,s} & 0 & 0 & -1 & 0 & 0 & 0 & 0 & 0\\
(\cdots)_{,s} & \mathbf{t}\times & 0 & 0 & 0 & -1 & 0 & 0 & 0 & 0\\
0 & 0 & -1 & 0 & -\bar{\mathbf{C}}_{\kappa} & 0 & 0 & 0 & 0 & 0\\
0 & 0 & 0 & -1 & 0 & -\bar{\mathbf{C}}_{\gamma} & 0 & 0 & 0 & 0\\
\hline
0 & 0 & 0 & 0 & 0 & 0 & 0 & 0 & 0 & 1\\
0 & 0 & 0 & 0 & 0 & 0 & 0 & 0 & 1 & 0\\
0 & 0 & 0 & 0 & 0 & 0 & 0 & 1 & 0 & 0\\
0 & 0 & 0 & 0 & 0 & 0 & 1 & 0 & 0 & 0
\end{array}\right]\left\{\begin{array}{c}\bar{\mathbf{u}}\\ \bar{\boldsymbol{\Omega}}\\ \bar{\mathbf{M}}\\ \bar{\mathbf{T}}\\ \bar{\boldsymbol{\kappa}}\\ \bar{\boldsymbol{\gamma}}\\ \bar{\mathbf{u}}_o\\ \bar{\boldsymbol{\Omega}}_o\\ \bar{\mathbf{M}}_o\\ \bar{\mathbf{T}}_o\end{array}\right\}-\left\{\begin{array}{c}\bar{\mathbf{q}}\\ \bar{\mathbf{m}}\\ \mathbf{0}\\ \mathbf{0}\\ \mathbf{0}\\ \mathbf{0}\\ \hat{\bar{\mathbf{T}}}_o\\ \hat{\bar{\mathbf{M}}}_o\\ \hat{\bar{\boldsymbol{\Omega}}}_o\\ \hat{\bar{\mathbf{u}}}_o\end{array}\right\} \tag{4.19}$$

If the operator is potential, the equality $\left\langle \mathrm{d}\mathbf{Q}\left(\mathbf{y},\bar{\mathbf{y}}\right),\mathbf{y}^{*}\right\rangle=\left\langle \mathrm{d}\mathbf{Q}\left(\mathbf{y},\mathbf{y}^{*}\right),\bar{\mathbf{y}}\right\rangle$ must be satisfied (Oden and Reddy, 1976). $\mathrm{d}\mathbf{Q}(\mathbf{y},\bar{\mathbf{y}})$ and $\mathrm{d}\mathbf{Q}(\mathbf{y},\mathbf{y}^{*})$ are Gâteaux derivatives of the operator in directions of $\bar{\mathbf{y}}$ and $\mathbf{y}^{*}$. Since the operator is potential then the functional corresponding to the field equations are obtained as follows:

$$\bar{\mathbf{I}}(\bar{\mathbf{y}}) = -\left[\bar{\mathbf{u}}, \frac{\mathrm{d}\bar{\mathbf{T}}}{\mathrm{d}s}\right] + \left[\mathbf{t}\times\bar{\mathbf{\Omega}}, \bar{\mathbf{T}}\right] - \left[\frac{\mathrm{d}\bar{\mathbf{M}}}{\mathrm{d}s}, \bar{\mathbf{\Omega}}\right] - \frac{1}{2}[\bar{\mathbf{C}}_{\kappa}\bar{\mathbf{M}}, \bar{\mathbf{M}}] - \frac{1}{2}[\bar{\mathbf{C}}_{\gamma}\bar{\mathbf{T}}, \bar{\mathbf{T}}]$$

$$+\frac{1}{2}\rho A z^2 [\bar{\mathbf{u}}, \bar{\mathbf{u}}] + \frac{1}{2}\rho z^2 \left[\mathbf{I}\bar{\mathbf{\Omega}}, \bar{\mathbf{\Omega}}\right] - [\bar{\mathbf{q}}, \bar{\mathbf{u}}] - [\bar{\mathbf{m}}, \bar{\mathbf{\Omega}}]$$

$$+\left[(\bar{\mathbf{T}} - \hat{\bar{\mathbf{T}}}), \bar{\mathbf{u}}\right]_{\sigma} + \left[(\bar{\mathbf{M}} - \hat{\bar{\mathbf{M}}}), \bar{\mathbf{\Omega}}\right]_{\sigma} + \left[\hat{\bar{\mathbf{u}}}, \bar{\mathbf{T}}\right]_{\varepsilon} + \left[\hat{\bar{\mathbf{\Omega}}}, \bar{\mathbf{M}}\right]_{\varepsilon} \qquad \textbf{(4.20)}$$

The terms with hats in the Eqn. **(4.20)** are known values on the boundary the subscripts, ε and σ represent the geometric and dynamic boundary conditions, respectively. Rotary inertia and shear influence terms are considered in the functional form (Arıbaş 2012., Eratlı *et al*. 2014).

4.5 Finite Element Formulation

Dimensionless coordinate are used in finite element derivation and the linear shape functions are $\phi_i = 1-\xi$ and $\phi_j = \xi$ (where $\xi = (\varphi - \varphi_i)/\Delta\varphi$, $0 < \xi < 1$, $\Delta\varphi = (\varphi_j - \varphi_i)$). The subscripts represent node numbers of the bar element $\varphi_j \rangle \varphi_i$. The element has two nodes with 2×12 degrees of freedom. In this study, exact function Eqns. **(4.2)**, **(4.3)** are used in the derivation of arc length curvature and torsion (c, χ, τ) (see Eqn. **(4.6)**). The total variables for the element matrix per node in the frequency domain is given as follows.

$$\bar{u}_t, \bar{u}_n, \bar{u}_b, \bar{\Omega}_t, \bar{\Omega}_n, \bar{\Omega}_b, \bar{T}_t, \bar{T}_n, \bar{T}_b, \bar{M}_t, \bar{M}_n, \bar{M}_b \qquad \textbf{(4.21)}$$

These variables in Eqn. (4.21) are defined by using interpolation function in the element. Namely,

$$\bar{u}_t^e = \bar{u}_{t1}^e \phi_1 + \bar{u}_{t2}^e \phi_2 \qquad \textbf{(4.22)}$$

where the superscript "*e*" denotes the element number. Variable cross-sections and different rigidities in Eqn. **(4.20)** are defined by using interpolating function. For example,

$$\begin{aligned} A^e &= A_1^e \phi_1 + A_2^e \phi_2 \\ \mathbf{I}^e &= \mathbf{I}_1^e \phi_1 + \mathbf{I}_2^e \phi_2 \\ \bar{\mathbf{C}}_{\gamma}^e &= \bar{\mathbf{C}}_{\gamma 1}^e \phi_1 + \bar{\mathbf{C}}_{\gamma 2}^e \phi_2 \\ \bar{\mathbf{C}}_{\kappa}^e &= \bar{\mathbf{C}}_{\kappa 1}^e \phi_1 + \bar{\mathbf{C}}_{\kappa 2}^e \phi_2 \end{aligned} \qquad \textbf{(4.23)}$$

External loads and moments are expressed as follows

$$\begin{aligned} \overline{\mathbf{q}}^{e} &= \overline{\mathbf{q}}_{1}^{e}\,\phi_{1} + \overline{\mathbf{q}}_{2}^{e}\,\phi_{2} \\ \overline{\mathbf{m}}^{e} &= \overline{\mathbf{m}}_{1}^{e}\,\phi_{1} + \overline{\mathbf{m}}_{2}^{e}\,\phi_{2} \end{aligned} \tag{4.24}$$

All expressions in Eqns. **(4.21)**, **(4.22)**, **(4.23)**, **(4.24)** are inserted into Eqn. **(4.20)**, and after classical finite element formulation procedure, the element matrix is derived. During the mathematical operations the following general form of the submatrices are used, namely:

$$[k_1] = \int_0^L \phi_i\,\phi_j\,\mathrm{d}s$$

$$[k_2] = \int_0^L \phi_i\,\phi_{j,s}\,\mathrm{d}s$$

$$[k_3]^{f} = \int_0^L (\,f_1\phi_1 + f_2\,\phi_2\,)\,\phi_i\,\phi_j\,\mathrm{d}s$$

$$[k_4]^{\kappa} = \int_0^L \frac{R(\theta)}{c^2(\theta)}\,\phi_i\,\phi_j\,\mathrm{d}s$$

$$[k_5]^{\tau} = \int_0^L \frac{h(\theta)}{c^2(\theta)}\,\phi_i\,\phi_j\,\mathrm{d}s$$

where $i, j = 1, 2$. The subscripts i and j of the shape functions shows node numbers of the bar element and also represents the row and column numbers of the terms of submatrices. L is the arc length of finite element, f defines variable cross sectional properties. The load vector terms are

$$\begin{aligned} \{k_6\}^{\overline{q}} &= \int_0^L \begin{Bmatrix} (\,\overline{q}_1\phi_1 + \overline{q}_2\,\phi_2\,)\,\phi_1 \\ (\,\overline{q}_1\phi_1 + \overline{q}_2\,\phi_2\,)\,\phi_2 \end{Bmatrix} \mathrm{d}s \\ \{k_6\}^{\overline{m}} &= \int_0^L \begin{Bmatrix} (\,\overline{m}_1\phi_1 + \overline{m}_2\,\phi_2\,)\,\phi_1 \\ (\,\overline{m}_1\phi_1 + \overline{m}_2\,\phi_2\,)\,\phi_2 \end{Bmatrix} \mathrm{d}s \end{aligned} \tag{4.25}$$

4.5.1 Matrices of element and external loads for barrel and hyperboloidal helix

Radius function $R(\xi) = a_1\,\xi^2 + a_2\,\xi + a_3$ of barrel and hyperboloidal helix (see Fig. 4.1) in Eqn. **(4.2)** are defined by using dimensionless coordinate

$$
\begin{aligned}
a_1 &= \frac{(R_2 - R_1)(\Delta\varphi)^2}{(\pi n)^2} \\
a_2 &= -\frac{2(R_2 - R_1)\Delta\varphi}{\pi n} + \frac{2(R_2 - R_1)\varphi_1 \Delta\varphi}{(\pi n)^2} \\
a_3 &= R_2 - \frac{2(R_2 - R_1)\varphi_1}{\pi n} + \frac{(R_2 - R_1)(\varphi_1)^2}{(\pi n)^2}
\end{aligned}
\tag{4.26}
$$

where, φ_1 is angle at first node of finite element. The submatrices of element matrice are as follows;

$$
[k_1] = \frac{B\Delta\varphi}{60}\begin{bmatrix} \{2a_1 + 5a_2 + 20a_3\} & \{3a_1 + 5a_2 + 10a_3\} \\ \{3a_1 + 5a_2 + 10a_3\} & \{12a_1 + 15a_2 + 20a_3\} \end{bmatrix} \tag{4.27}
$$

$$
[k_2] = \begin{bmatrix} -0.5 & 0.5 \\ -0.5 & 0.5 \end{bmatrix} \tag{4.28}
$$

$$
[k_3]^f = \frac{B\Delta\varphi}{60}\begin{bmatrix} A_{11} & A_{12} \\ A_{21} & A_{22} \end{bmatrix} \tag{4.29}
$$

$$
[k_4]^\kappa = \frac{\Delta\varphi}{3B}\begin{bmatrix} 1 & 0.5 \\ 0.5 & 1 \end{bmatrix} \tag{4.30}
$$

$$
[k_5]^\tau = \frac{\Delta\varphi}{3B'}\begin{bmatrix} 1 & 0.5 \\ 0.5 & 1 \end{bmatrix} \tag{4.31}
$$

$$
\left.\begin{aligned} B &= \sqrt{1 + \tan^2\alpha} \\ B' &= \frac{B}{\tan\alpha} \end{aligned}\right\} \tag{4.32}
$$

where

$$
\begin{aligned}
A_{11} &= f_1(a_1 + 3a_2 + 15a_3) + f_2(a_1 + 2a_2 + 5a_3) \\
A_{12} &= A_{21} = f_1(a_1 + 2a_2 + 5a_3) + f_2(2a_1 + 3a_2 + 5a_3) \\
A_{22} &= f_1(2a_1 + 3a_2 + 5a_3) + f_2(10a_1 + 12a_2 + 15a_3)
\end{aligned}
\tag{4.33}
$$

For (4.29) f is either of one $\bar{C}_\kappa^t, \bar{C}_\kappa^n, \bar{C}_\kappa^b, \bar{C}_\gamma^t, \bar{C}_\gamma^n, \bar{C}_\gamma^b$ or A, I_t, I_n, I_b in (4.33).

4.5.2 Matrices of element and external loads for conical helix

Radius function $R(\xi)=e_1+e_2\,\xi$ of conical helix (see Fig. **4.1**) in Eqn. **(4.3)** are defined by using dimensionless coordinate

$$\begin{aligned} e_1 &= R_1+\frac{(R_2-R_1)}{2\pi n}\varphi_1 \\ e_2 &= \frac{(R_2-R_1)\Delta\varphi}{2\pi n} \end{aligned} \tag{4.34}$$

where, φ_1 is angle at first node of finite element. The submatrices of element matrice are as follows;

$$[k_1]=\frac{B\,\Delta\varphi}{12}\begin{bmatrix} \{\,4e_1+e_2\,\} & \{\,2e_1+e_2\,\} \\ \{\,2e_1+e_2\,\} & \{\,4e_1+3e_2\,\} \end{bmatrix} \tag{4.35}$$

$$[k_3]^f=\frac{B\,\Delta\varphi}{60}\begin{bmatrix} E_{11} & E_{12} \\ E_{21} & E_{22} \end{bmatrix} \tag{4.36}$$

where

$$\begin{aligned} E_{11} &= 3f_1(\,5e_1+e_2)+f_2(\,5e_1+2e_2) \\ E_{12} &= E_{21}=f_1(\,5e_1+2e_2)+f_2(5e_1+3e_2) \\ E_{22} &= f_1(\,5e_1+2e_2)+3f_2(5e_1+4e_2) \end{aligned} \tag{4.37}$$

For Eqn. **(4.36)** f is either of one $\bar{C}^t_\kappa,\bar{C}^n_\kappa,\bar{C}^b_\kappa,\bar{C}^t_\gamma,\bar{C}^n_\gamma,\bar{C}^b_\gamma$ or A,I_t,I_n,I_b in Eqn. **(4.37)**. Please note that, $[k_2]$, $[k_4]^\kappa$, $[k_5]^\tau$, B, B' are as defined in section 4.5.1

5. NON-CYLINDRICAL HELICAL BARS

5.1 Verification Analysis - Elastic Analysis

The objective of this section is to verify new curvature formulation inserted into the present finite element program which was developed in ITU by Omurtag M.H in 1990. We will show that, by this formulation exact curvatures of non-cylindrical helical geometries are simulated in a more precise way. For the verification, the free vibration analysis of non- cylindrical elastic helical bars, *e.g*. hyperboloidal, barrel and conical, are handled.

5.1.1 Example 1.1 : The hyperboloidal helical bar

An elastic hyperboloidal helical bar, having circular cross section and fixed at both ends is solved. The material and geometrical properties are:

the modulus of elasticity	:	$E = 210\,\text{GPa}$
Poisson's ratio	:	$\upsilon = 0.3$
the material density	:	$\rho = 7850\,\text{kg/m}^3$
the number of active turns	:	$n = 6.5$
pitch angle	:	$\alpha = 4.8°$
the ratio of major radius to minor radius	:	$R_2 / R_1 = 2.4$, and $R_1 = 13\,\text{mm}$
circular cross section radius	:	$r = 1.3\,\text{mm}$

The first five natural frequencies of the hyperboloidal helix are calculated using different meshes and convergence results are shown in Table 5.1. The results are compared with Lee (2007), and SAP 2000 (750 elements and the number of unknowns: 4506) in Table 5.2. The Convergence of the present element is excellent even with a coarse mesh. Through the rest of the solutions 150 elements (the number of unknowns:1812) are used. The convergence of the first two frequencies with Lee (2007), Yıldırım (1997) and SAP2000 for are shown graphically in Fig. 5.1. In this

example, the shear correction factor $k' = 1.18$ is used (Omurtag 2013). The value of shear correction factor is considered $k' = 1.1$ in J. Lee (2007) and Yıldırım (1997).

Table 5.1 : The convergence result of the element for the first five frequencies (Hz) for the hyperboloidal helical bar (n_e :number of elements).

Modes	This study n_e				
	50	100	150	200	250
1	75.64	75.75	75.76	75.76	75.76
2	95.76	96.28	96.31	96.31	96.31
3	100.85	102.95	103.06	103.07	103.08
4	132.58	133.2	133.23	133.23	133.23
5	160.5	160.71	160.72	160.72	160.72

Table 5.2 : The first five frequencies (Hz) for the hyperboloidal helical bar ($\text{diff.\%} = (\text{This study} - \text{Ref}) \times 100 / \text{This study}$).

Modes	This study $n_e = 150$	Lee 2007	diff.%	SAP2000 $n_e = 750$	diff.%
1	75.76	75.76	0.00	75.65	0.15
2	96.31	96.31	0.00	95.57	0.77
3	103.06	103.09	-0.03	103.36	-0.29
4	133.23	133.21	0.02	132.49	0.56
5	160.72	160.70	0.01	159.56	0.72

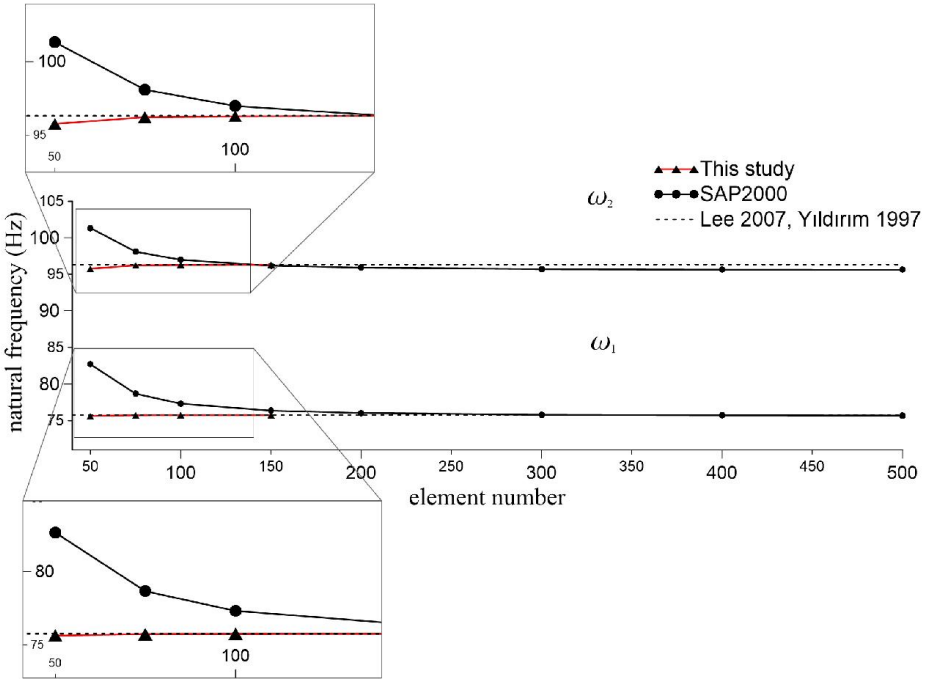

Figure 5.1 : The first two frequencies graph for the hyperboloidal helical bar.

5.1.2 Example 1.2 : The barrel helical bar

A barrel helix bar, having circular cross section and fixed at both ends is solved. The material and geometrical properties are:

the modulus of elasticity	:	$E = 210\,\text{GPa}$
Poisson's ratio	:	$\upsilon = 0.3$
the material density	:	$\rho = 7850\,\text{kg/m}^3$
the number of active turns	:	$n = 6.5$
pitch angle	:	$\alpha = 4.8°$
the ratio of minor radius to major radius	:	$R_2 / R_1 = 0.4$, and $R_1 = 25\,\text{mm}$
circular cross section radius	:	$r = 1\,\text{mm}$

The first five natural frequencies of the barrel helix are calculated using different meshes and convergence results are shown in Table 5.3.The results are compared with Lee (2007), and SAP 2000 (750 elements the number of unknowns:4506) in Table 5.4. The Convergence of the present element is excellent even with a coarse mesh. Through the rest of the solutions 150 elements (the number of unknowns:1812) are used. The convergence of the first two frequencies with Lee (2007), Yıldırım (1997) and SAP2000 are shown graphically in Fig. 5.2 . In this example, the shear correction factor $k' = 1.18$ is used (Omurtag 2013). The value of shear correction factor is considered $k' = 1.1$ in J. Lee (2007) and Yıldırım (1997).

Table 5.3 : The convergence result of first five frequencies (Hz) for the barrel helical bar (n_e :number of elements).

Modes	This study n_e				
	50	75	100	150	250
1	65.30	65.54	65.54	65.54	65.54
2	71.51	71.51	71.51	71.51	71.51
3	85.31	86.63	86.84	86.91	86.93
4	85.38	86.70	86.91	86.98	87.00
5	129.59	129.59	129.59	129.59	129.59

Table 5.4 : The first five frequencies (Hz) for the barrel helical bar (diff.%:(This study − Ref)×100 / This study).

Modes	This study $n_e = 150$	Lee 2007	diff.%	SAP2000 $n_e = 750$	diff.%
1	65.54	65.53	0.02	65.70	-0.24
2	71.51	71.52	-0.01	71.86	-0.49
3	86.91	86.93	-0.02	87.14	-0.26
4	86.98	87.00	-0.02	87.21	-0.26
5	129.59	129.60	-0.01	130.19	-0.46

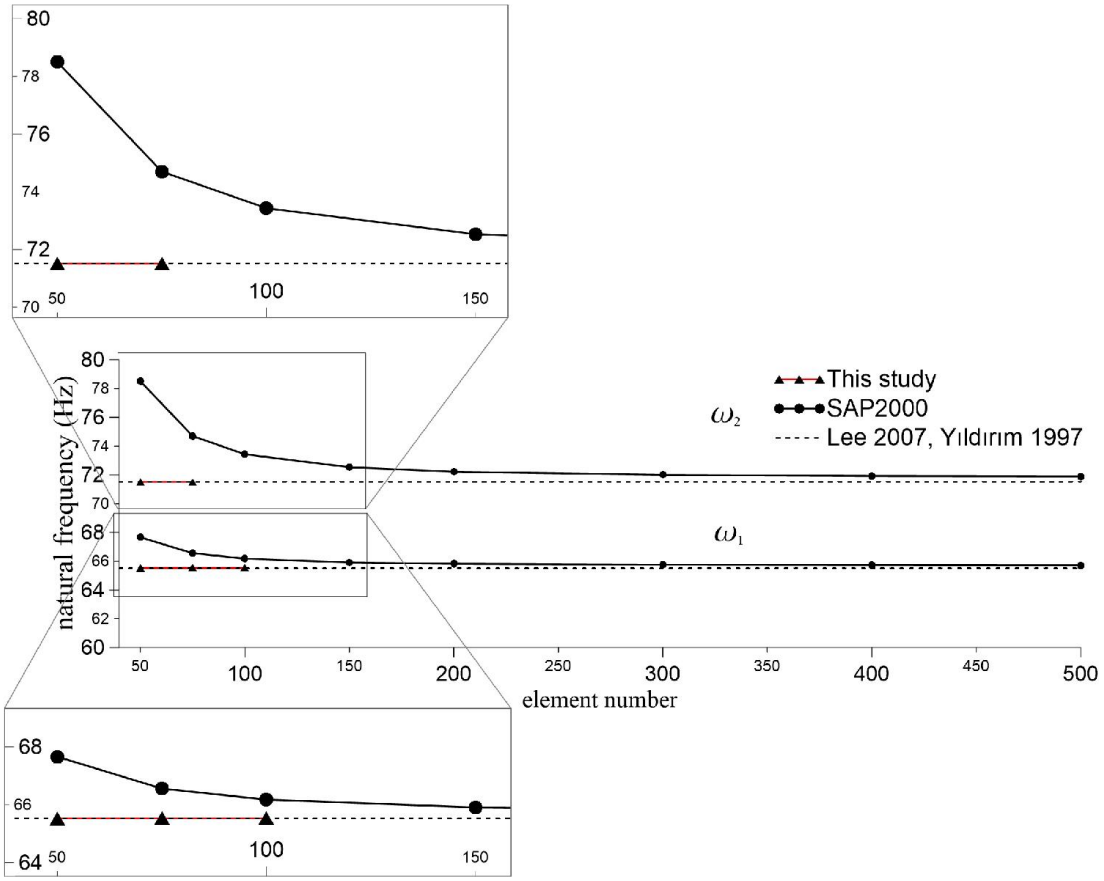

Figure 5.2 : The first two frequencies graph for the barrel helical bar.

5.1.3 Example 1.3 : The conical helical bar

A conical helix bar, having circular cross section and fixed at both ends is solved. The material and geometrical properties are:

the modulus of elasticity : $E = 206.1\text{GPa}$

Poisson's ratio : $\upsilon = 0.3$

the material density : $\rho = 7900\,\text{kg/m}^3$

the number of active turns : $n = 7.6$

pitch angle : $\alpha = 8.5744°$

the ratio of minor radius to major radius : $R_2 / R_1 = 0.5$, and $R_1 = 5\,\text{mm}$

circular cross section radius : $r = 0.5\,\text{mm}$

The first six natural frequencies of the conical helix are calculated using different meshes and convergence results are shown in Table 5.5. The results are compared with Lee (2007), and SAP 2000 (750 elements and the number of unknowns:4506) in Table 5.6. The Convergence of the present element is excellent even with a coarse mesh. Through the rest of the solutions 250 elements (the number of unknowns:3012) are used. The convergence of the first two frequencies with Lee (2007), Yıldırım (2004) and SAP2000 for are shown graphically in Fig. 5.3. In this example, the shear correction factor $k' = 1.18$ is used (Omurtag 2013).The value of shear correction factor is considered $k' = 1.1$ in J. Lee (2007) and Yıldırım (2004).

Table 5.5 : The convergence result of first six frequencies (Hz) for the conical helical bar (n_e :number of elements).

Modes	This study n_e					
	50	75	100	150	250	350
1	654.91	679.43	683.13	684.45	684.72	684.76
2	658.05	683.28	687.08	688.43	688.72	688.75
3	815.37	815.72	815.79	815.82	815.82	815.82
4	878.57	879.63	879.80	879.86	879.88	879.87
5	1419.07	1457.83	1463.37	1465.31	1465.73	1465.77
6	1441.17	1484.16	1490.16	1492.62	1492.72	1492.77

Table 5.6 : The first six frequencies (Hz) for the conical helical bar.

(diff.%:$\left(\text{This study-Ref}\right)\times 100$ / This study).

Modes	This study $n_e = 250$	Lee 2007	diff.%	SAP2000 $n_e = 750$	diff.%
1	684.72	684.76	-0.01	684.72	0.00
2	688.72	688.76	-0.01	688.68	0.01
3	815.82	816.06	-0.03	816.33	-0.06
4	879.88	879.38	0.06	880.76	-0.10
5	1465.73	1465.50	0.02	1466.56	-0.06
6	1492.72	1492.70	0.00	1493.38	-0.04

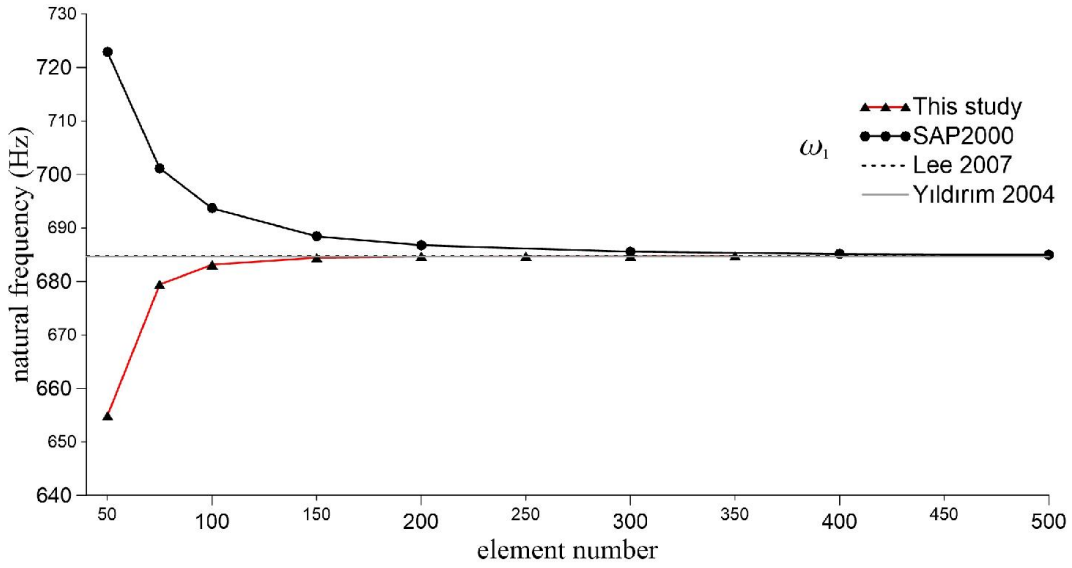

(a) The first frequency graph for the conical helix.

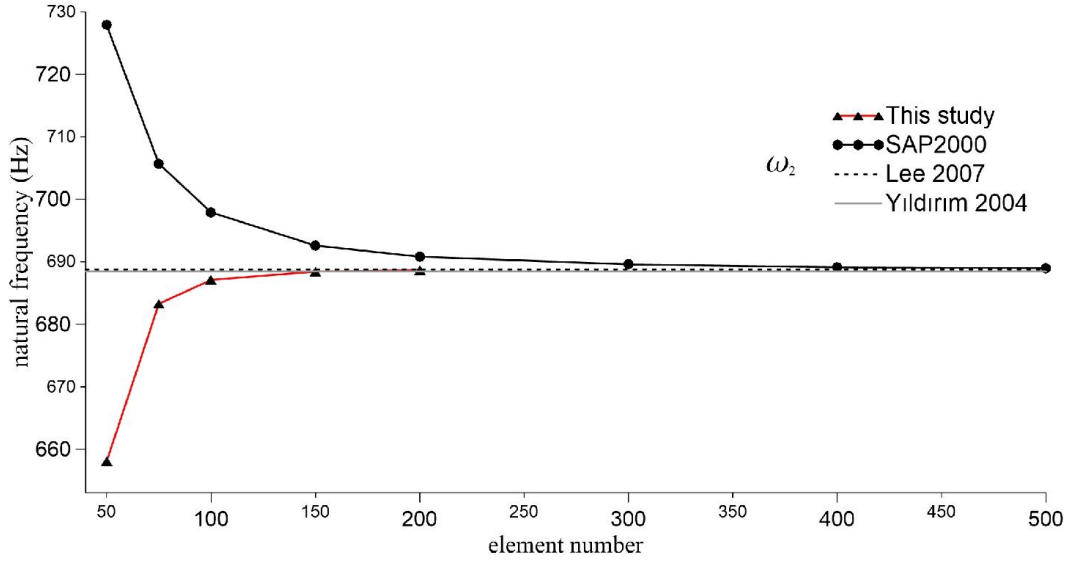

(b) The second frequency graph for the conical helical bar.

Figure 5.3 : The first two frequencies graph for the conical helical bar.

5.1.4 Example 1.4 : Shear correction factor and Poisson's ratio

Shear coefficient is defined as a function of Poisson's ratio by Cowper (1966) as follows,

Hollow circular section

$$K = \frac{6(1+\upsilon)(1+m^2)^2}{7(1+6\upsilon)(1+m^2)^2+(20+12\upsilon)}, \quad m = \frac{r_{inner}}{r_{outer}} \tag{5.1}$$

Thin-walled hollow circular

$$K = \frac{2(1+\upsilon)}{4+3\upsilon} \tag{5.2}$$

It is related by shear correction factor by,

$$k' = \frac{1}{K} \tag{5.3}$$

In this example, we are interested with the influence the shear correction factor and on the first five natural frequencies, which is calculated over the Poisson's ratio (see Eqn. **(5.1)** and Eqn.**(5.2)**). A unique helix geometry is solved for two different cross-sections, namely hollow circular section and thin-walled hollow circular. Two different shear correction factors are used, one is for $\upsilon = 0$ and the other for $\upsilon = 0.3$. The natural angular frequency results are compared with each other. An elastic cantilever hyperboloidal helical bar is handled. The common material geometrical properties of the helical bar are as follow:

the shear modulus	:	$G = 80\,\text{GPa}$
Poisson's ratio	:	$\upsilon = 0.3$
the material density	:	$\rho = 7850\ \text{kg/m}^3$
the height of helix	:	$H = 4\text{m}$
the ratio of minor radius to major radius	:	$R_1 / R_2 = 0.5$, where $R_2 = 2\,\text{m}$
the number of active turn	:	$n = 6$
the net area for all cross-sections	:	$A = 153.94\,\text{cm}^2$
the number of element	:	$n_e = 200$

The inner and the outer radius of the hollow circular cross section are $r_{inner} = 5.25\,\text{cm}$ and $r_{outer} = 8.75\,\text{cm}$, repectively. The shear correction factor is calculated by using the formula in Eqn. **(5.1)** and Eqn.**(5.3)**, as follows

$$k'_0 = K^{-1}(\upsilon = 0, m = 0.6) = 1.82 \tag{5.4}$$

$$k'_{0.3} = K^{-1}(\upsilon = 0.3, m = 0.6) = 1.72 \tag{5.5}$$

where $m = r_{inner} / r_{outer} = 5.25 / 8.75 = 0.6$. The percent differenence between $k'_{0.3}$ and k'_0 (see Eqns. **(5.4)** and **(5.5)**)normalized with respect to k'_0 is 5.49%. The first five

natural frequency values corresponding to k_0' and $k_{0.3}'$, and the differenence between these two results normalized with respect to k_0' natural frequency results are given in Table (5.7).

Table 5.7 : The first five natural frequency values corresponding to k_0' and $k_{0.3}'$ of the hyperboloidal helical bar having hollow circular cross section.

Modes	Angular natural frequency (Hz)		diff.%
	for k_0'	for $k_{0.3}'$	
1	0.543517791	0.543531797	-0.00258
2	0.548102568	0.548115937	-0.00244
3	0.817358831	0.817460054	-0.01238
4	0.920840898	0.92084233	-0.00016
5	1.587267049	1.587351401	-0.00531

The inner and the outer radius of the thin-walled hollow circular cross section are $r_{inner} = 14.87\,\text{cm}$ and $r_{outer} = 16.435\,\text{cm}$, repectively. The shear correction factor is calculated by using the formula in Eqn. **(5.1)** and Eqn.**(5.3)**, as follows

$$k_0' = K^{-1}(\upsilon = 0) = 2 \qquad \textbf{(5.6)}$$

$$k_{0.3}' = K^{-1}(\upsilon = 0.3) = 1.88 \qquad \textbf{(5.7)}$$

The percent differenence between $k_{0.3}'$ and k_0' (see Eqns. **(5.6)** and **(5.7)**) normalized with respect to k_0' 6.00 %. The first five natural frequency values corresponding to k_0' and $k_{0.3}'$, and the differenence between these two results normalized with respect to k_0' natural frequency results are given in Table Table (5.8). Since the difference between the first five natural frequency values calculated by using k_0' and $k_{0.3}'$ are neglicable for both hollow circular and thin-walled hollow circular sections, for the rest of the examples only k_0' values are used for the respective sections.

Table 5.8 : The first five natural frequency values corresponding to k_0' and $k_{0.3}'$ of hyperboloidal helical bar having the thin-walled hollow circular cross section.

Modes	Angular natural frequency (Hz)		diff.%
	for k_0'	for $k_{0.3}'$	
1	1.176507876	1.176678490	-0.014502
2	1.186497236	1.186659574	-0.013682
3	1.758467793	1.759678803	-0.068867
4	1.994912514	1.994930499	-0.000902
5	3.422920215	3.423937851	-0.029730

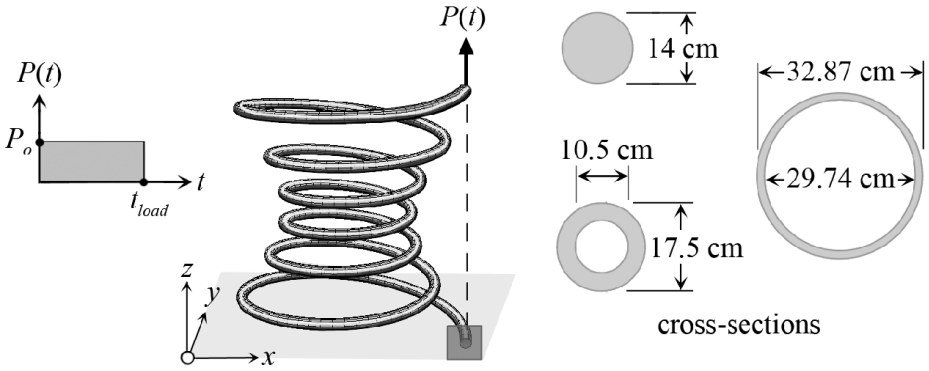

Figure 5.4 : Hyperboloidal helix geometry

5.2 Viscoelastic Analysis

The influence of the section geometry, the helix geometry and the effects of viscous shear modulus on the dynamic response of a viscoelastic cantilever hyperboloidal helical bar (see Figure 5.4) are investigated. The viscoelastic material exhibits the standard type of distortional behavior while having elastic Poisson's ratio $\overline{\upsilon} = \upsilon$. In the analyses, the common material geometrical properties of the helical bar are as follow:

the shear modulus	:	$G = 80\,\text{GPa}$
Poisson's ratio	:	$\upsilon = 0.3$
the material density	:	$\rho = 7850\ \text{kg/m}^3$
the height of helix	:	$H = 4\text{m}$
the ratio of minor radius to major radius	:	$R_1 / R_2 = 0.5$, where $R_2 = 2\,\text{m}$
the net area for all cross-sections	:	$A = 153.94\,\text{cm}^2$

The bar is subjected to a rectangular impulsive type of external dynamic load $P = P(t)$ acting from the free end of the bar as seen in Figure 1

the intensity of the loading	:	$P = 1000\,\text{N}$
the duration of the loading	:	$t_{load} = 50\,\text{s}$

The dynamic response of the bar is determined within $0 \le t \le 100\,\text{s}$. The analyses are carried out in the Laplace space and the results are transformed back to the time

space numerically by using modified Durbin's algorithms (Dubner 1974, Narayanan 1980). The parameters which are used in the analysis for inverse Laplace transformation algorithm are $N = 2^{11}$ and $aT = 6$ which are verified by Eratlı *et al.* (2014).

In the examples that follows, the time history curves of the displacements (u_x, u_z), the rotation Ω_y at the free end of the bar, and, the shear force T_z and the moment M_y at fixed end of the bar are determined. By using these curves (see Figures 5.5, 5.6, 5.7, 5.8, 5.9), the dynamic behavior of hyperboloidal helical bars having different material and geometrical properties are compared.

5.2.1 Example 3.1: The convergence analysis of a viscoelastic cantilever hyperboloidal helical bar

The solid-circular cross-sectional area is $A = 153.94\,\text{cm}^2$ and the shear correction factor $k' = 1.18$ is used (Omurtag 2013). For the convergence analysis the following parameters are selected:

the number of active turn of the helix : $n = 6$

the retardation time : $\tau_r^G = 0.01\text{s}$

the ratio associated with shear modulus : $\beta^G = 3$

The solutions are determined by discretizing the bar using 40, 60, 80 and 100 finite elements. The time histories for u_x, u_z, Ω_y and, T_z are given in Fig. 5.5, respectively. From the time variation curves (which are evaluated using 80 and 100 elements), the values of first six extrema (see Fig. 5.5) that occur within the forced vibration zone are determined. Absolute percent differences of these extrema values, belonging to the solutions determined using 80 and 100 elements, are evaluated and they are normalized with respect to the extrema values of 100 elements. The standard deviations of the normalized absolute percent differences for displacements (u_x, u_z), rotation Ω_y and shear force T_z are 0.807 ± 0.04, 0.648 ± 0.17, 0.985 ± 0.05 and 0.062 ± 0.06, respectively. As a consequence, in the solutions, 100 mixed elements are employed.

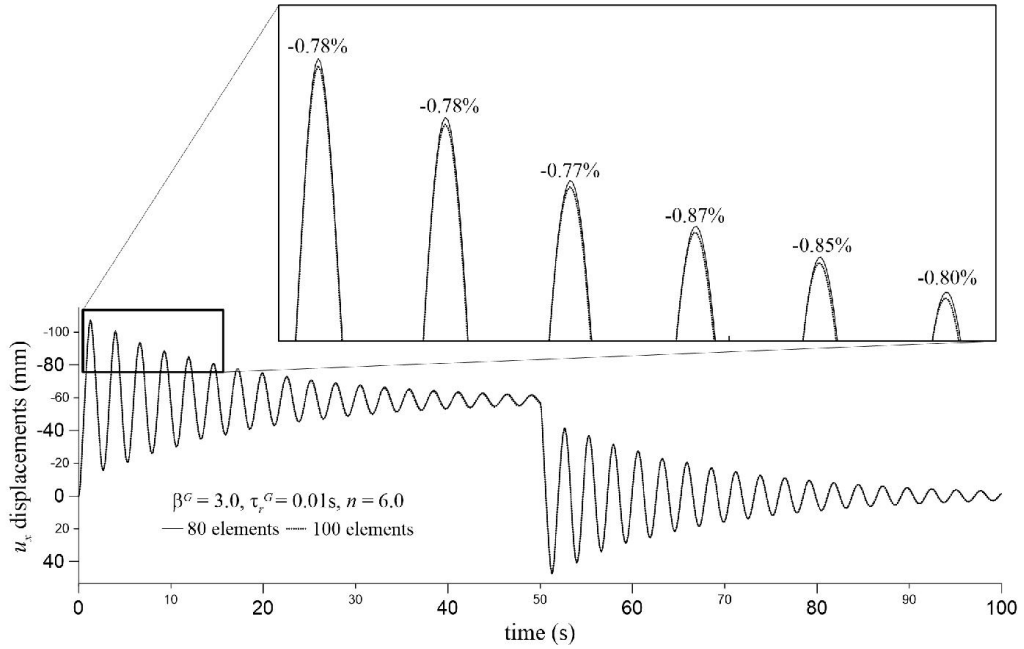

(a) The displacement u_x at the tip of the bar.

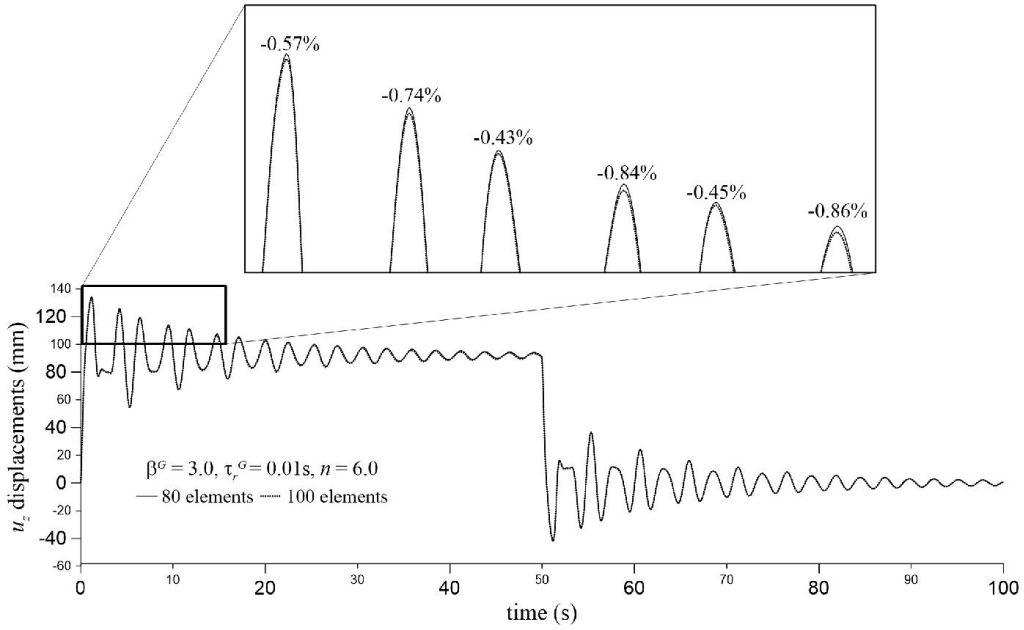

(b) The displacement u_z at the tip of the bar.

Figure 5.5 : The convergence test for a cantiliver hyperboloidal helical bar.

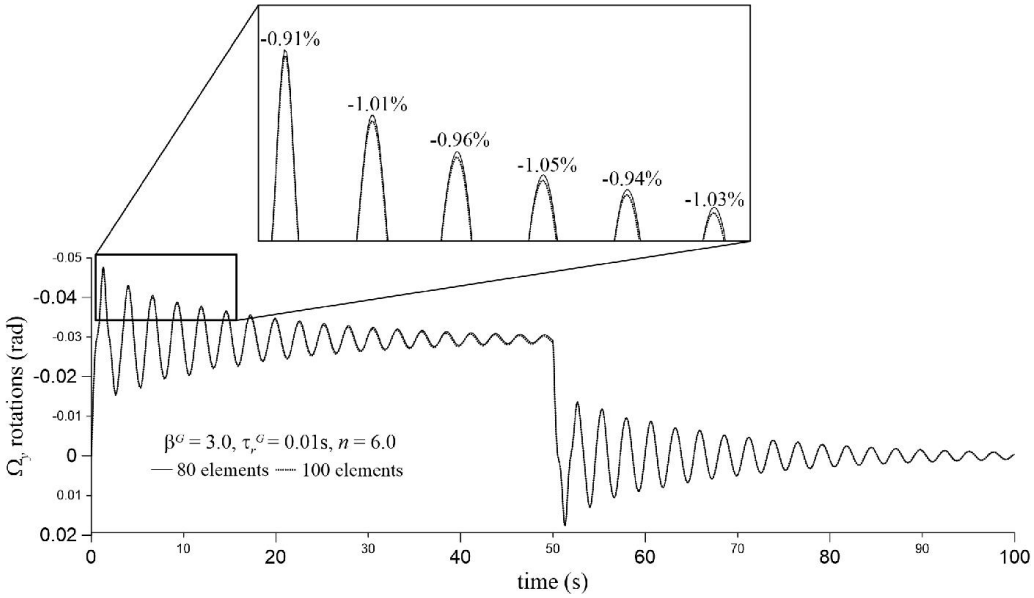

(c) The rotation Ω_y at the tip of the bar.

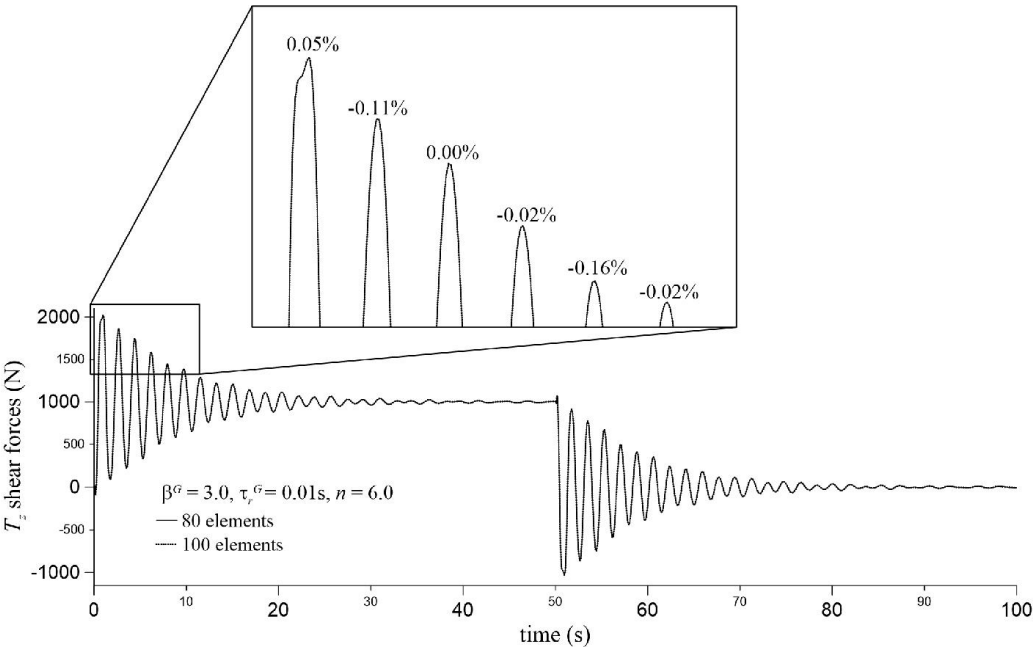

(d) The shear force T_z at the fixed end of the bar.

Figure 5.5(continued): The convergence test for a cantilever hyperboloidal helical bar.

5.3 Time histories of viscoelastic hyperboloidal helical bar

5.3.1 Example 3.2: The retardation time τ_r^G associated with the shear modulus

The solid-circular cross-sectional area is $A = 153.94\,\text{cm}^2$ and the shear correction factor $k' = 1.18$ is used (Omurtag 2013). and the viscoelastic material has different

values of retardation time $\tau_r^G = 0.005\text{s}, 0.01\text{s}, 0.1\text{s}$ (see Figure 5.6). The values of the parameters that describe the helix geometry, cross-section and the ratio associated with shear modulus β^G are the same with those used in the convergence analysis Sec. 5.2.1 .

the number of active turn of the bar : $n = 6$

the ratio associated with shear modulus : $\beta^G = 3$

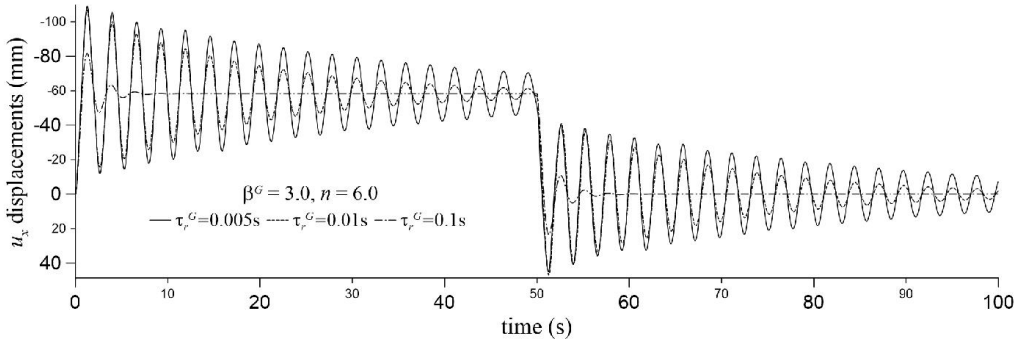

(a) the displacement u_x at the tip of the bar.

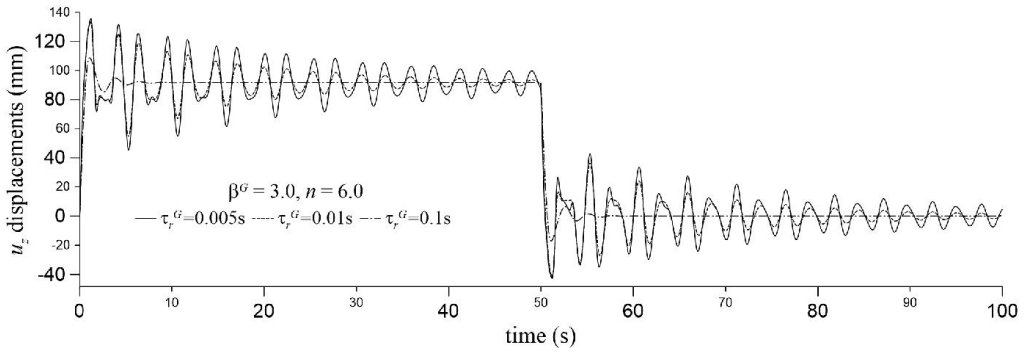

(b) the displacement u_z at the tip of the bar.

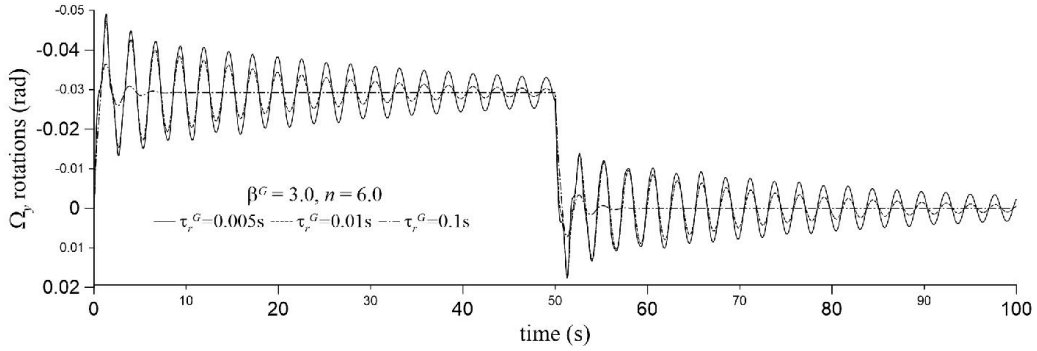

(c) the rotation Ω_y at the tip of the bar.

Figure 5.6 : Time histories of viscoelastic hyperboloidal helical bar for different values of retardation time τ_r^G associated with shear modulus.

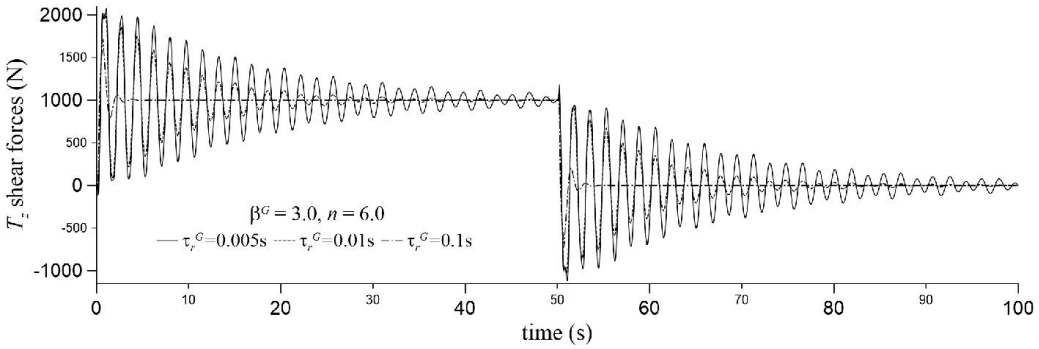

(d) the shear force T_z at the fixed end of the bar.

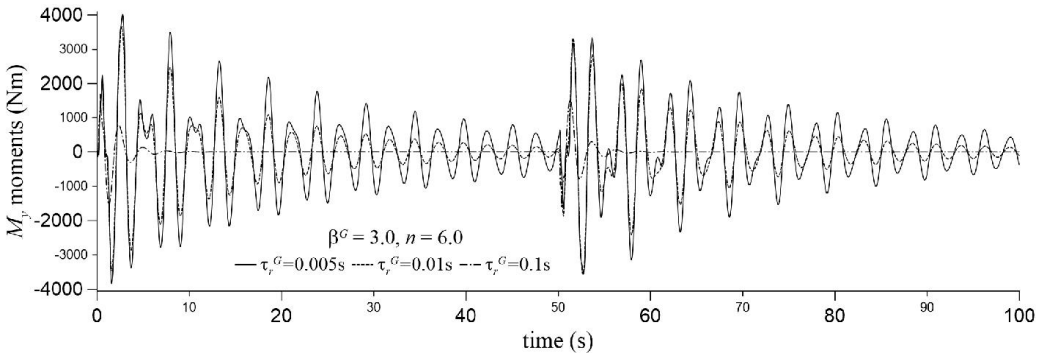

(e) the moment M_y at the fixed end of the bar.

Figure 5.6(continued): Time histories of viscoelastic hyperboloidal helical bar for different values of retardation time τ_r^G, associated with shear modulus.

5.3.2 Example 3.3: The ratio of β^G associated with shear modulus

The bars having different values of the ratio $\beta^G = 1.1, 1.5, 3.0$ associated with shear modulus are investigated (see Figure 5.7). The solid-circular cross-sectioned bar is considered having $A = 153.94\,\text{cm}^2$ and the shear correction factor $k' = 1.18$ is used (Omurtag 2013). The values of the parameters that describe the helix geometry, cross-section and the retardation time τ_r^G are the same with those used in the convergence analysis Sec. 5.2.1 .

the number of active turn of the bar : $n = 6$

the retardation time : $\tau_r^G = 0.01\text{s}$

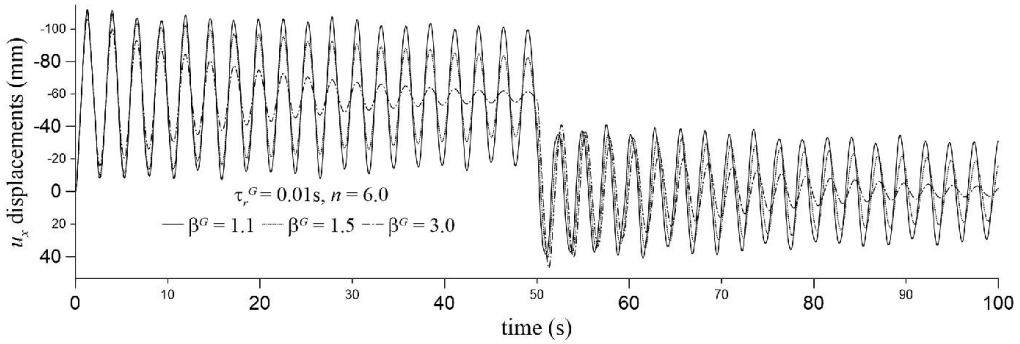

(a) the displacement u_x at the tip of the bar.

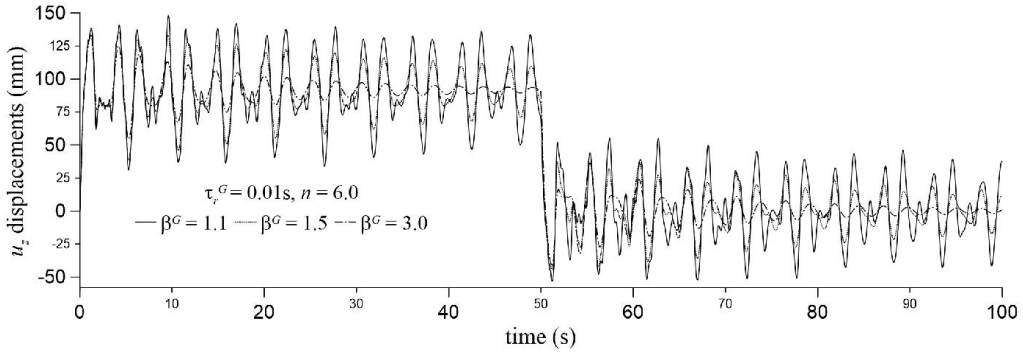

(b) the displacement u_z at the tip of the bar.

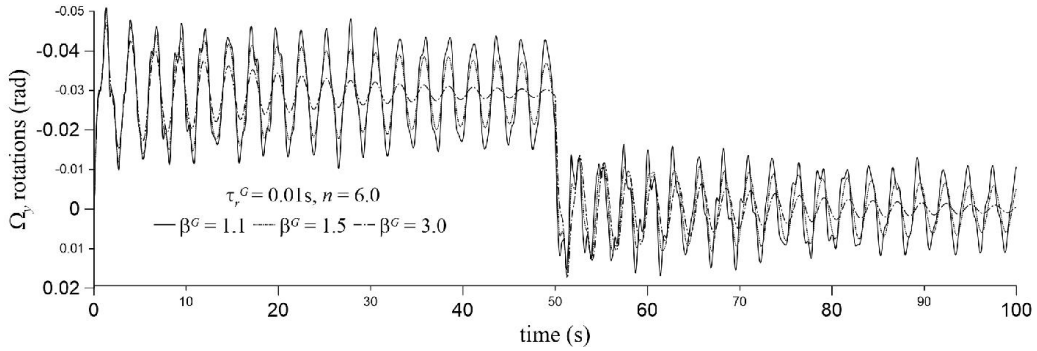

(c) the rotation Ω_y at the tip of the bar.

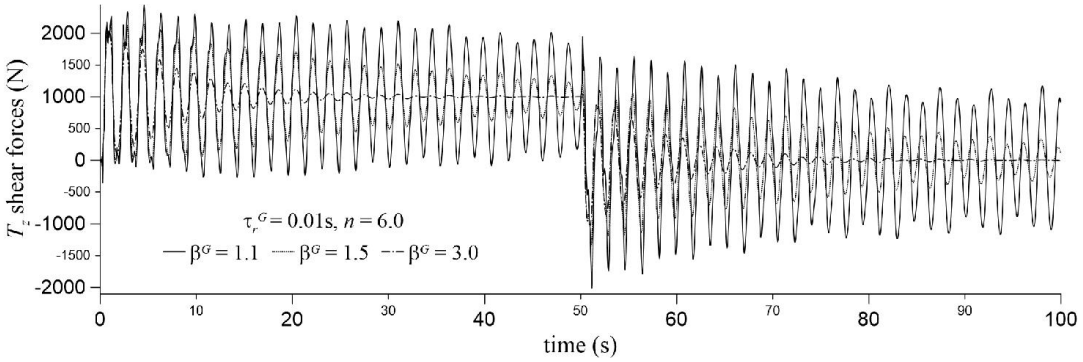

(d) the shear force T_z at the fixed end of the bar.

Figure 5.7 : Time histories of viscoelastic hyperboloidal helical bar for different values of β^G associated with shear modulus.

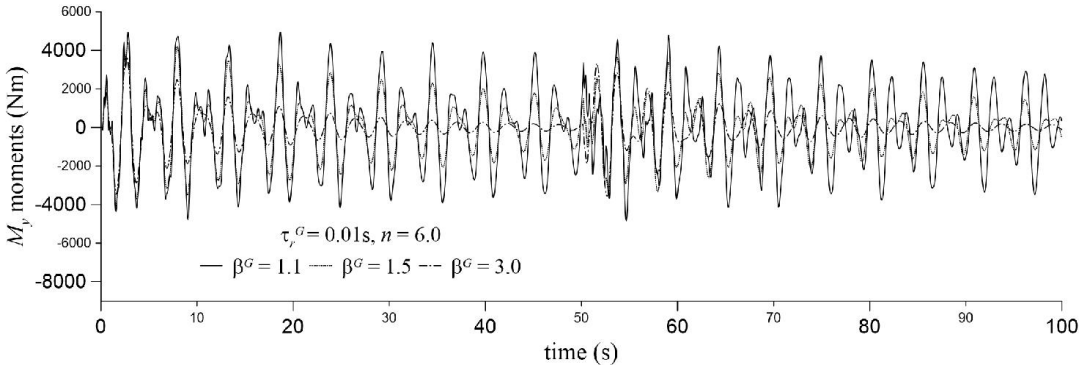

(e) the moment M_y at the fixed end of the bar.

Figure 5.7 (continued): Time histories of viscoelastic hyperboloidal helical bar for different values of β^G associated with shear modulus.

The influence of the parameters of viscoelastic material (τ_r^G, β^G) on the dynamic behavior are shown in Figures 5.6 and 5.7 by plotting the time histories of u_x, u_z, Ω_y, T_z and M_y. In Fig. 5.6, time histories are determined for $\tau_r^G = 0.005\text{s}, 0.01\text{s}, 0.1\text{s}$, $\beta^G = 3$, whereas, in Fig. 5.7 they are calculated for $\beta^G = 1.1, 1.5, 3.0$, $\tau_r^G = 0.01\text{s}$. We recall that, parameters τ_r^G and β^G describe the standard type of distortional behavior. From these two figures it is observed that, as the values of τ_r^G and β^G increase, u_x, u_z, Ω_y, T_z and M_y dissipate more rapidly, and, they also have smaller amplitudes. This behaviour is expected since the increase in the values of these parameters signifies that the distortional viscous behavior becomes more dominant in the material. It is also seen that, the change in the values of τ_r^G and β^G do not effect the vibration period.

5.3.3 Example 3.4 : For three different values of the number of active turns (n)

The bars having different number of active turns ($n = 2, 4, 6$) are investigated (see Figure 5.8). The solid-circular cross-sectioned bar is considered having $A = 153.94\,\text{cm}^2$ and the shear correction factor $k' = 1.18$ is used (Omurtag 2013). The values of the parameters that describe the helix geometry, cross-section, τ_r^G and β^G describe the standard type of distortional behavior are the same with those used in the convergence analysis

the retardation time : $\tau_r^G = 0.01\text{s}$

the ratio associated with shear modulus : $\beta^G = 3$

From Figure 5.8, we see that, as n increases, u_x, u_z, Ω_y oscillate about larger values (absolutely) in the forced vibration zone. More clearly, in the forced vibration zone for the values of $n = 2, 4, 6$, the oscillations are about $-17.5\,\text{mm}$, $-38\,\text{mm}$, $-57.8\,\text{mm}$ for u_x, $26.1\,\text{mm}$, $59.3\,\text{mm}$, $92.2\,\text{mm}$ for u_z and $-0.01\,\text{rad}$, $-0.02\,\text{rad}$, $-0.03\,\text{rad}$ for Ω_y. On the other hand, T_z and M_y oscillate about 1000 N and 0 in the forced vibration zone for all values of n (*e.g.* Figure 5.8d, Figure 5.8e). From the time variation curves, it is also observed that, as n decreases, all the responses damp more rapidly while their amplitude and vibration period decrease.

From the time variation curves (which are evaluated for $n = 2, 4, 6$), the values of first six extrema (see Fig.5.8) that occur within the forced vibration zone are determined. Absolute percent differences between these values are evaluated and normalized with respect to $n = 6$. The standard deviations of the nodal values are obtained. The comparison for u_x, u_z and Ω_y with the results that correspond to $n = 6$ indicates that the reductions in the case of $n = 2$ are 76.618 ± 0.663, 74.792 ± 0.810 and 75.070 ± 0.348, in the case of $n = 4$ are 39.998 ± 1.113, 38.61 ± 2.426 and 38.863 ± 0.829, respectively.

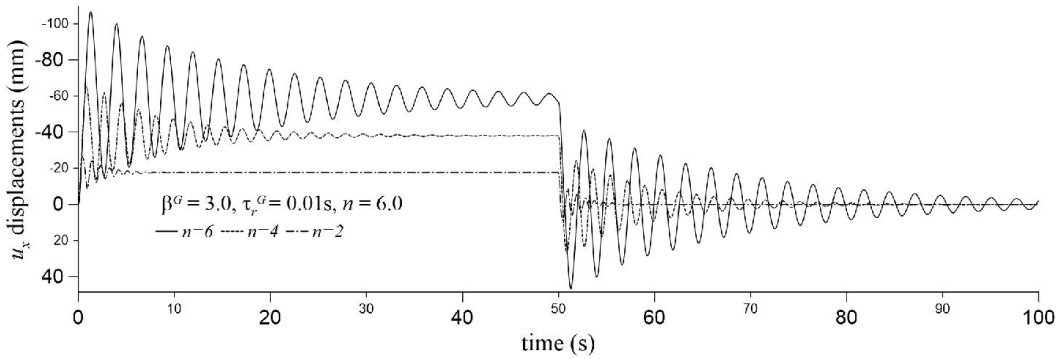

(a) the displacement u_x at the tip of the bar.

Figure 5.8 : Time histories of viscoelastic hyperboloidal helical bar for different values of the number of active turns (n).

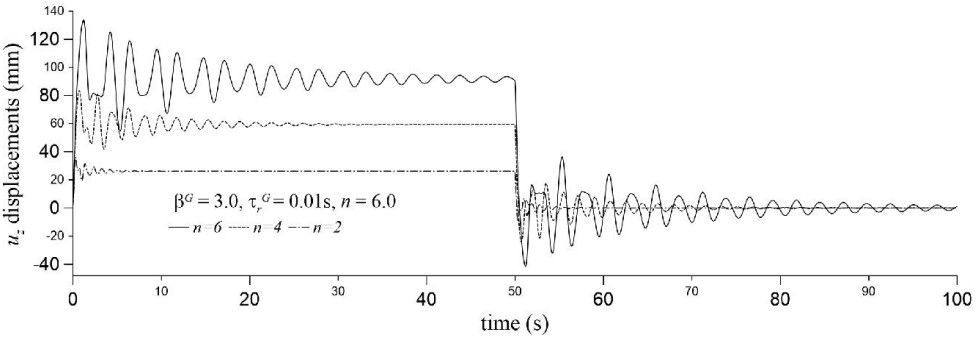

(b) the displacement u_z at the tip of the bar.

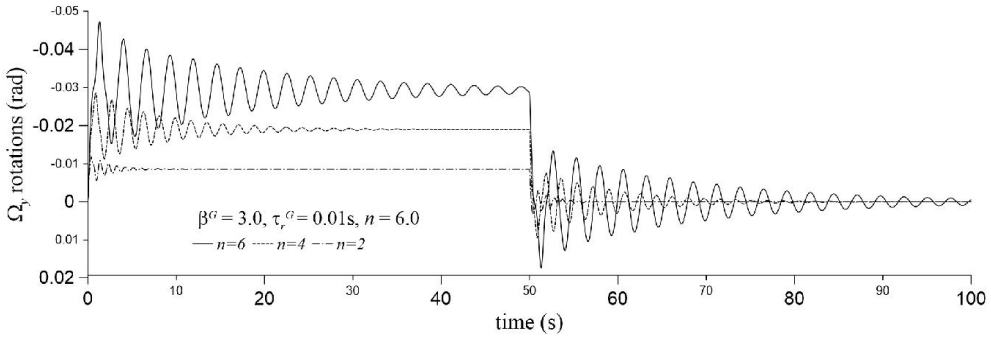

(c) the rotation Ω_y at the tip of the bar.

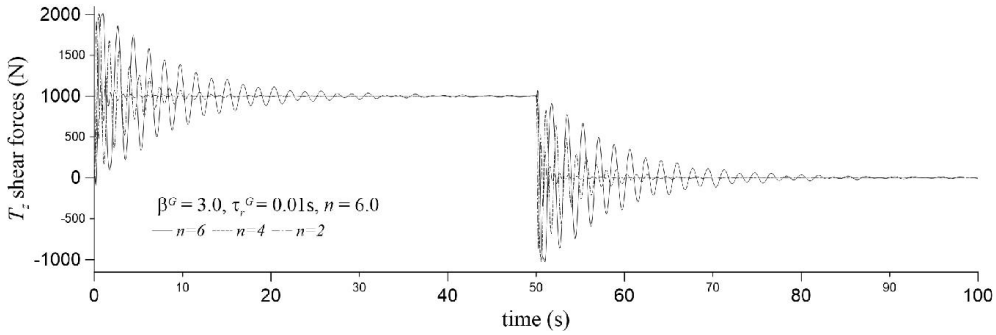

(d) the shear force T_z at the fixed end of the bar.

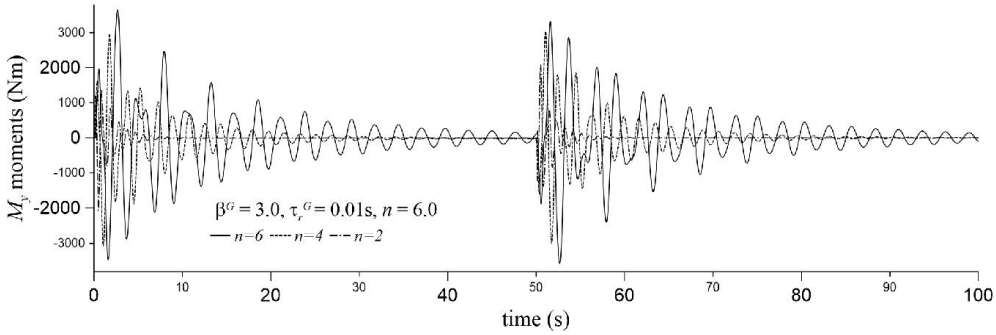

(e) the moment M_y at the fixed end of the bar.

Figure 5.8 (continued): Time histories of viscoelastic hyperboloidal helical bar for different values of the number of active turns (n).

5.3.4 Example 3.5 : Three different types of the cross-sections

The differences between dynamic behaviors of bars having different cross-sectional shapes (see Fig. 5.4) are examined. The bars having solid-circular, hollow-circular and thin-walled hollow-circular cross-sections are considered (see Fig. 5.9). The net cross-sectional area for each type of cross-section is taken as $A = 153.94\,\text{cm}^2$. The shear correction factors $k^{'}$ are taken as following cross sections:

the solid circular type	:	$k' = 1.18$	(Omurtag 2013).
the hollow circular type	:	$k' = 1.82$	(Cowper 1966).
the thin-walled hollow-circular type	:	$k' = 2$	(Cowper 1966).

The values of the parameters that describe the helix geometry, cross-section, τ_r^G and β^G describe the standard type of distortional behavior are the same with those used in the convergence analysis

the retardation time	:	$\tau_r^G = 0.01\text{s}$
the ratio associated with shear modulus	:	$\beta^G = 3$

Figure 5.9 shows, the time variations of the selected quantities. It is seen that, the time variations are significantly affected from shape of the cross-sections. In the forced vibration zone for solid-circular, hollow-circular and thin-walled hollow-circular bars, the oscillations are about $-58.3\,\text{mm}$, $-27.4\,\text{mm}$, $-5.8\,\text{mm}$ for u_x, $91.2\,\text{mm}$, $43.1\,\text{mm}$, $9.21\,\text{mm}$ for u_z and $-0.03\,\text{rad}$, $-0.01\,\text{rad}$, $-0.003\,\text{rad}$ for Ω_y. The responses determined for thin-walled hollow-circular bar damp very rapidly, and the vibration period and amplitude of these responses are very low valued when compared with the others. Within the three bars, thin-walled hollow-circular bar turns out to be the most stiff, while the opposite behavior is true for the solid-circular bar.

From the time variation curves (which are evaluated for circular, hollow circle, thin-walled circular hollow,), the values of first six extrema (see Fig.5.9) that occur within the forced vibration zone are determined. Absolute percent differences between these values are evaluated and normalized with respect to solid-circular cross-section. The standard deviations of the nodal values are obtained. The comparison for u_x , u_z and

Ω_y with the results that correspond to the solid-circular cross-section indicates that the reductions in the case of the hollow-circular are 55.796 ± 1.098, 54.837 ± 0.624 and 55.118 ± 0.532, in the case of the thin-walled hollow-circular are 91.947 ± 0.549, 91.159 ± 0.315 and 91.484 ± 0.223, respectively.

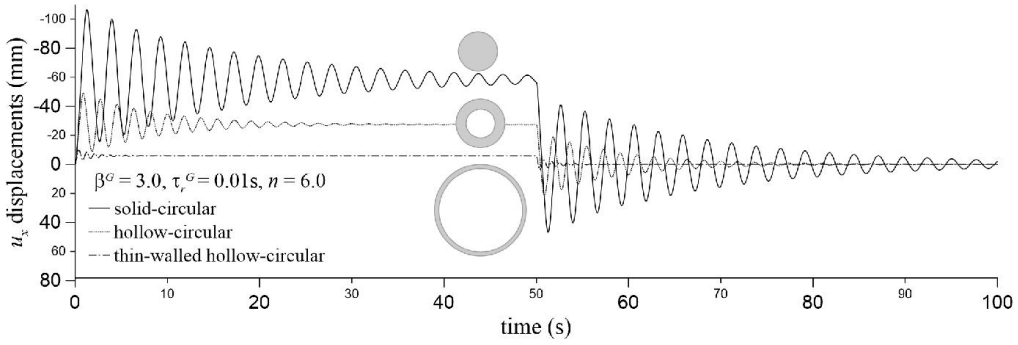

(a) the displacement u_x at the tip of the bar.

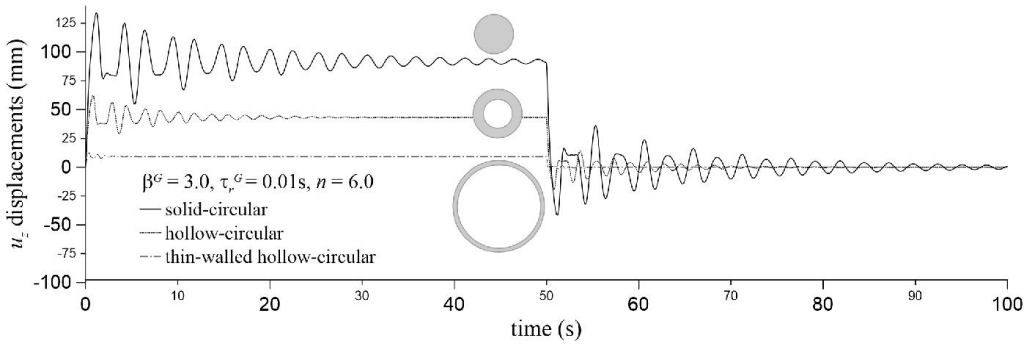

(b) the displacement u_z at the tip of the bar.

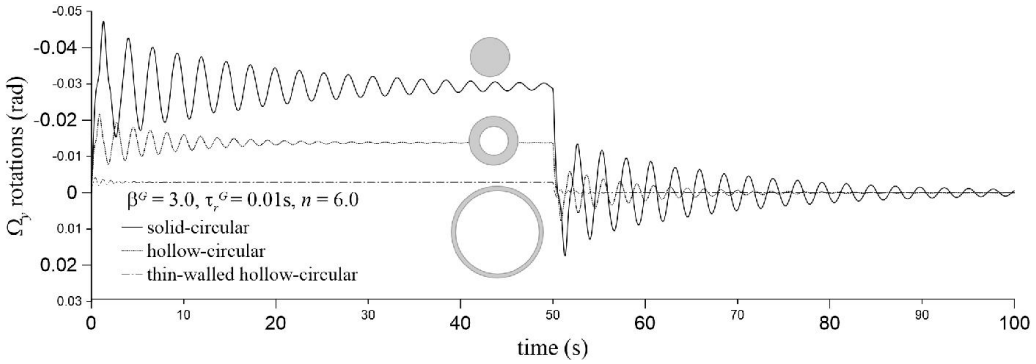

(c) the rotation Ω_y at the tip of the bar.

Figure 5.9 : Time histories of viscoelastic hyperboloidal helical bar for three different types of the cross-section.

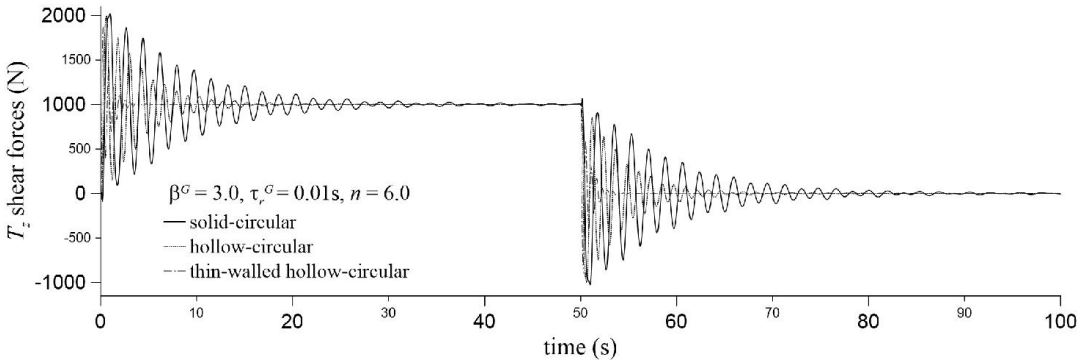

(d) the shear force T_z at the fixed end of the bar.

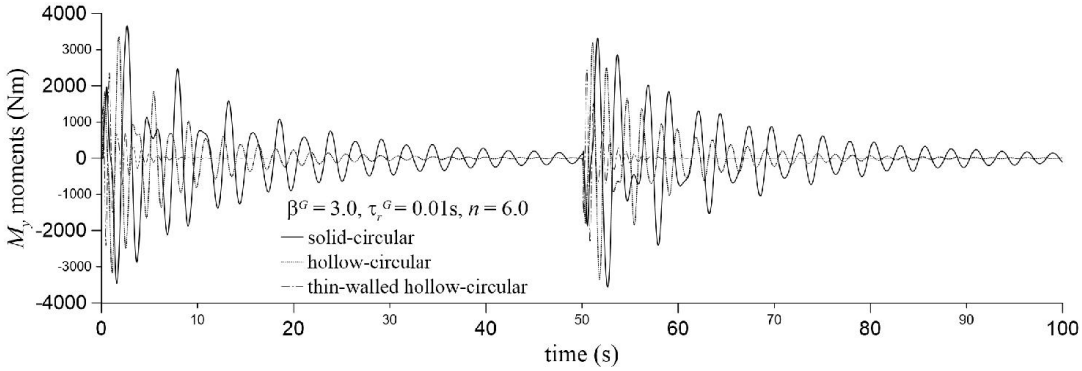

(e) the moment M_y at the fixed end of the bar.

Figure 5.9 (continued): Time histories of viscoelastic hyperboloidal helical bar for three different types of the cross-section.

6. RESULTS AND DISCUSSION

In this thesis, using the exact expressions of defined the helix geometry properties a new mixed finite element formulation is obtained and it is verified by the free vibration analysis of elastic hyperboloidal, barrel and conical helical bars under fixed-fixed boundary conditions. The Timoshenko theory is employed and two nodded curved element is used. It is assumed that, the linear viscoelastic material exhibits standard type of distortional behavior while having elastic Poisson's ratio and the material properties are implemented into the formulation through the use of the correspondence principle. The finite element solution is carried out in the Laplace space, and then the results are transformed back to the time space numerically via Modified Durbin's transformation algorithm (Eratlı *et al.* 2014). As a viscoelastic analysis, the dynamic behavior of a cantilevered viscoelastic hyperboloidal helical bar under rectangular impulsive type of loading is solved as an original problem is handled.

The following remarks can be given for the elastic non-cylindrical helical bars, respectively:

- In order to verify the new geometry definition of the element, the non-cylindrical elastic helical bars existing in the literature and the results of a commercial finite element program SAP2000 are handled, and quite satisfactory results are obtained. The element fast in convergence even with a coarse meshing (see Figure 5.1, Figure 5.2, Figure 5.3)

The influence the shear correction factor is investigated on the first five natural frequency values, which is calculated over the Poisson's ratio for a elastic cantiliver hyperboloidal bar. The analyses is performed the two different shear correction factors are used, one is for $\upsilon = 0$ and the other for $\upsilon = 0.3$. Since the difference between the first five natural frequency values calculated by using k_0' and $k_{0.3}'$ are neglicable for both hollow circular and thin-walled hollow circular sections, for the rest of the examples only k_0' values are used for the respective sections.

As benchmark examples, keeping shear modulus, Poisson's ratio, the material density, the height of helix, the ratio of minor radius to major radius, the net area for all cross-sections as constant, the intensity of loading and the duration of loading nine different viscoelastic hyperboloidal helical bars are analyzed and the following remarks can be given:

- Through the analysis, a convergence analysis is performed for 40, 60, 80 and 100 finite elements. It is observed that results of 80 and 100 finite elements are quite satisfactory (see Figure 5.5). As a consequence, in the solutions, through the rest of the numerical analysis 100 elements is employed.
- The influence of the viscous shear modulus on the dynamic response due to various number of active turns and the cross-sectional shape of the bar is as follows:
    - Increasing the values of τ_r^G and β^G, increased the dissipation rate of the displacements (u_x, u_z), rotation (Ω_y), shear force (T_z) and moment (M_y) (see Figure 5.6 and 5.7).
    - The magnitudes of the displacements and rotations decreased due to the decreasing number of active turns (see Figure 5.8).
    - The magnitudes of the displacements and rotations are decreased if the hollow-circular cross-section is replaced by the solid circular (see Figure 5.9).
    - The period of the vibrations decreased if the hollow-circular cross-section is replaced by the solid circular (see Figure 5.9).
    - The magnitudes of the displacements and rotations are considerably decreased if the thin-walled hollow-circular cross-section is replaced by the solid circular (see Figure 5.9).
    - The period of the vibrations considerably decreased if the thin-walled hollow-circular cross-section is replaced by the solid circular (see Figure 5.9).

- As a verification, T_z and M_y oscillate about 1000 N and 0 in the forced vibration zone for the all dynamic analyses (see Figures 5.6, 5.7, 5.8, 5.9).

REFERENCES

Aköz, Y., Kadıoğlu, F. (1999). The Mixed finite element method for the quasi-static and dynamic analysis of viscoelastic Timoshenko beams, *Int. J. Numer. Meth. Eng., 44*, 1909-1932.

Aldemir, Ü., Aydın, E. (2005). New approaches on design of earthquake resistant structures, (in Turkish), *TMH – Turkey Engineering News, 435,* 81-86.

Alfrey, T. (1948). *Mechanical Behavior of High Polymers*. New York: Interscience.

Arıbaş, Ü.N. (2012). *Analysis of dynamic behavior of viscoelastic helicoidal rods with mixed finite element method* (Master's thesis). Istanbul Technical University, Istanbul, Turkey.

Baranoglu, B., Mengi, Y. (2006). The use of dual reciprocity boundary element method in coupled thermoviscoelasticity, *Computer Methods in Applied Mech. and Eng*, *196* , 379-392.

Boley, B.A., Weiner, J.H. (1960). *Theory of Thermal Stresses*. New York: John Wiley & Sons Inc.

Brigham, E.O. (1974). *The Fast Fourier Transform*. Englewood Cliffs, N.J.: Prentice Hall Inc.

Busool, W., Eisenberger, M. (2002). Free vibration of helicoidal beams of arbitrary shape and variable cross section. *J. Vib. Acoust., 124*, 397-409.

Cebecigil, E. (2005). *Quasi-static analysis of viscoelastic Timoshenko beams on Winkler foundation using the mixed finite element method* (Master's Thesis, in Turkish. Istanbul Technical University, Istanbul, Turkey.

Chen, W.H., Lin, T.C. (1982). Dynamic Analysis of viscoelastic structure using incremental finite element method. *Engineering Structures, 4*, 271-276.

Christensen, R.M. (1982). *Theory of viscoelasticity: an introduction* (2nd ed.). New York: Academic Press.

Cowper, G. R. (1966) The Shear Coefficient in timoshenko's Beam Theory. *Journal of Applied Mechanics*, *33* , 335-340.

Çalım, F.F. (2003). *Dynamic analysis of viscoelastic, anisotropic curved spatial rod systems* (Doctoral dissertation), in Turkish. Çukurova University, Adana, Turkey.

Çalım, F.F. (2009a). Dynamic analysis of composite coil springs of arbitrary shape. *Composites: Part B, 40,* 741-757.

Çalım, F.F. (2009b). Forced vibration of helical rods of arbitrary shape. *Mechanics Research Communications, 36,* 882-891.

Çalım, F.F., Temel, B. (2002). Dynamic behaviors of viscoelastic straight rods, (in Turkish), *Journal of Faculty of Engineering and Architecture of Cukurova University, 17(1-2),* 59-69.

Dubner, H., Abate, J. (1968). Numerical inversion of Laplace transforms by relating them to the finite Fourier cosine transform. *Journal of the Association for Computing Mechinary, 15(1),* 115-123.

Durbin, F. (1974). Numerical inversion of Laplace transforms: An efficient improvement to Dubner and Abate's Method. *Computer Journal, 17,* 371-376.

Eratlı, N., Argeso, H., Çalım, F.F., Temel, B., Omurtag, M.H. (2014) Dynamic analysis of linear viscoelastic cylindrical and conical helicoidal rods using the mixed FEM, *J. Sound Vib, 333,* 3671–3690.

Findley, W., Lai, J.S., Onaran, K. (1976). *Creep and Relaxation of Nonlinear Viscoelastic Material*. New York: North-Holland.

Flügge, W. (1975). *Viscoelasticity*. New York: Springer-Verlag.

Girgin, K. (2006). Free vibration analysis of non-cylindrical helices with variable cross-section by using mixed FEM. *J. Sound Vib., 297,* 931-945.

Kadıoğlu, F. (1999). *Quasi-static and dynamic analysis of viscoelastic rods* (Doctoral dissertation), in Turkish. Istanbul Technical University, Istanbul, Turkey.

Kadıoğlu, F., Aköz, Y. (2003). The mixed finite element method for quasi-static and dynamic analysis of viscoelastic circular beams, *Struct. Eng. Mech., 15(6)*, 735-752.

Kıral, E., Tokdemir, S., Ural, S. (1976). Transient response of an elastic or/and viscoelastic curved rod under arbitrary time dependent loading, *METU J. Pure and Applied Sciences, 9,* 63-86.

Kocatürk, T., Şimşek, M. (2004). Vibration of viscoelastic beams subjected to moving harmonic loads. *J. Engng. and Natural Sciences, 3,* 116-128.

Kocatürk, T., Şimşek, M. (2006a). Dynamic Analysis of Eccentrically Prestressed Viscoelastic Timoshenko Beams Under a Moving Harmonic Load. *Computers and Structures, 84(31-32),* 2113-2127.

Kocatürk, T., Şimşek, M. (2006b). Vibration of viscoelastic beams subjected to an eccentric compressive force and a concentrated moving harmonic force. *J. Sound Vib., 291(1-2),* 302-322.

Lee, E.H. (1955). Stress analysis in viscoelastic bodies, *Q. Appl. Math., 13,* 183-190.

Lee, J. (2007). Free vibration analysis of non-cylindrical helical springs by the pseudospectral method. *J. Sound Vib., 305,* 543-551.

Mengi Y., Argeso H. (2006) A unified approach for the formulation of interaction problems by the boundary element method, *Int. J. Numer. Methods Eng.*, *66*, 816-842.

Nagaya, K., Takeda, S., Nakata, Y. (1986). Free vibration of coil springs of arbitrary shape. *Int. J. Numer. Meth. Eng., 23,* 1081-1099.

Narayanan, G.V. (1980). *Numerical Operational Methods in Structural Dynamics* (Doctoral dissertation). University of Minnesota, Mineapolis, America.

Oden, J.T., Reddy, J.N. (1976). *An introduction to the mathematical theory of finite elements*. New York: John Wiley & Sons Inc.

Olgun, O. (2004). *Static and Dynamic analysis of helicoidal bars with mixed finite element method* (Master's thesis), in Turkish. Istanbul Technical University, Istanbul, Turkey.

Omurtag, M.H. (1990). *Solution of the reinforced cylindrical shells with variable cross-section by using mixed finite element method* (Doctoral dissertation), in Turkish. Istanbul Technical University, Istanbul, Turkey.

Omurtag, M.H. (2013).*Mukavemet Cilt 2* ,3. Edition,Publisher*:* Birsen, İstanbul.

Omurtag, M.H., Aköz, A.Y. (1992). The mixed finite element solution of helical beams with variable cross-section under arbitrary loading. *Comput. and Struct., 43(2),* 325-331.

Payette, G.S., Reddy, J.N. (2010). Nonlinear quasi-static finite element formulations for viscoelastic Euler-Bernoulli and Timoshenko beams. *Int. J. Numer. Meth. Biomed. Engng., 26,* 1736-1755.

Read, W.T. (1950). Stress analysis for compressible viscoelastic materials, *J. Appl. Phys., 21,* 671-674.

Shames, I.R. and Cozarelli, F.A. (1997). *Elastic and Inelastic Stress Analysis*, CRC Press Inc. United States.

Spiegel, Murray R. (1965). *Theory and Problems of Laplace Transforms,* SCHAUM'S Outline Series, McGraw-Hill. Singapore.

Temel, B. (2004). Transient Analysis of Viscoelastic Helical Rods Subject to Time-Dependent Loads. *J. Sound Vib., 41(5-6),* 1605-1624.

Temel, B., Çalım, F.F. (2003). Forced vibration of cylindrical helical rods subjected to impulsive loads. *J. Appl. Mech., 70,* 281-291.

Temel, B., Çalım, F.F., Baran, T. (2003). Behavior of viscoelastic straight planar rods that have variable cross-sections subject to dynamic external load and ground motion, (in Turkish), *Journal of Faculty of Engineering and Architecture of Cukurova University, 18(2),* 101-114.

Temel, B., Çalım, F.F., Tütüncü, N. (2004). Quasi-Static and Dynamic Response of Viscoelastic Helical Rods. *J. Sound Vib., 271(3-5),* 921-935.

Temel, B., Çalım, F.F., Tütüncü, N. (2005). Forced vibration of composite cylindrical helical rods. *Int. J. Mech. Sci., 47,* 998-1022.

Tezcan, S.S., Uluca, O. (2003). Reduction of earthquake response of plane frame buildings by viscoelastic dampers. *Eng. Struct., 25,* 1755-1761.

Tsien, H.S. (1950). A generalization of Alfrey's theorem for viscoelastic media, *Q. Appl. Math., 8,* 104-106.

White, J.L., (1968). Finite element in linear viscoelasticity. *Proceeding 2nd Conference on Matrix Method in Structural Mechnanics*, Ohio:

Wright-Patterson Air Force Base. 15-17 October (AFFDL-TR-68-150).

Yamada, Y., Takabatake, H., Sato, T. (1974). Effect of time-dependent material properties on dynamic response. *Int. J. Numer. Meth. Eng., 8,* 403-414.

Yıldırım, V. (1997). Free vibration analysis of non-cylindrical coil springs by combined use of the transfer matrix and the complementary functions methods. *Commun. Numer. Meth. Eng., 13,* 487-494.

Yıldırım, V. (1998). A parametric study on the free vibration of non-cylindrical helical springs. *J. Appl. Mech. ASME, 65,* 157-163.

Yıldırım, V. (1999). A numerical study on the free vibration of symmetric cross-ply laminated cylindrical helical springs. *Transactions of the ASME, 66,* 1040-1043.

Yıldırım, V. (2001a). Free vibration of uniaxial composite cylindrical helical springs with circular cross-section. *J. Sound Vib., 239(2),* 321-333.

Yıldırım, V. (2001b). Free vibration characteristics of composite barrel and hyperboloidal coil springs. *Mech. Composite Material and Struc., 8,* 205-217.

Yıldırım, V. (2002). Expressions for predicting fundamental natural frequencies of non-cylindrical helical springs. *J. Sound Vib., 252(3),* 479-491.

Yıldırım, V. (2004). A parametric study on the natural frequencies of unidirectional composite conical springs. *Commun. Numer. Meth. Eng., 20,* 207-227.

Yıldırım, V., İnce, N. (1997). Natural frequencies of helical springs of arbitrary shape. *J. Sound Vib., 204(2),* 311-329.

Yıldırım, V., Sancaktar, E. (2000). Linear free vibration analysis of cross-ply laminated cylindrical helical springs. *Int. J. Mech. Sci., 42,* 1153-1169.

Yıldırım, V., Sancaktar, E., Kıral, E. (1999). The effect of the longitudinal to transverse moduli ratio on the natural frequencies of symmetric cross-ply laminated cylindrical helical springs. *Transactions of the ASME, Journal of Mechanical Design, 121,* 634-639.

Yükseloğlu, B. (2005). *Dynamic analysis of viscoelastic Timoshenko beams on Winkler foundation using the mixed finite element method* (Master's thesis), in Turkish. Istanbul Technical University, Istanbul, Turkey.

CURRICULUM VITAE

Name Surname:	**Merve ERMİŞ**
Place and Date of Birth:	**İstanbul, 27.02.1989**
e-mail:	**merve.civileng@gmail.com**
B.Sc.:	**Yıldız Technical University**
	Mathematical Engineering (2006-2011)
	Civil Engineering (2008-2012) (Double major)
M.Sc.:	**Istanbul Technical University (2012-2015)**

List of Publications and Patents:

▪ **Ermiş M.,** Eratlı N., Omurtag M.H., 2013. The free vibration analysis of elastic helices having thin and thick walled box cross section, (in Turkish). *Proceedings 18. National Mechanics Congress*, August 26-30, Manisa, Turkey.

▪ **Ermiş M.**, Eratlı N., Omurtag M. H., 2014. Static and dynamic analysis of elastic cylindrical helixes with arbitrary cross-sections by using the mixed finite element method, *ACE 2014- 11th Internatıonal Congress On Advances In Civil Engineering*, October 20-25, Istanbul, Turkey.

▪ **Ermiş M.**, Eratlı N., Argeso H., Çalım F.F., Omurtag M.H., 2014. Quasi-static and dynamic analyses of viscoelastic conical helixes with a squared box cross-section, *ACE 2014- 11th Internatıonal Congress On Advances In Civil Engineering*, October 20-25, Istanbul, Turkey.

▪ Eratlı N., **Ermiş M**., Omurtag M.H., 2015. Free vibration analysis of helicoidal bars with thin-walled circular tube cross-section via mixed finite element method, *Sigma Journal of Engineering and Natural Sciences*, Vol 33(2) 200-218.

▪ **PUBLICATIONS/PRESENTATIONS ON THE THESIS**

▪ **Ermiş M.,** Eratlı N., Omurtag M.H., 2015. The Influence of the Rotary Inertia on the Dynamic Behavior of Viscoelastic Non-cylindrical Helicoidal Bars, *ICCMSE 2015- 11th International Conference of Computational Methods in*

Sciences and Engineering, March 20-23, Athens, Greece.

▪ **Ermiş M.,** Eratlı N., Argeso H., Omurtag M.H., 2015. The Effects of the Viscous Bulk Compressibility for Cantilevered Cylindrical Helices Bars, *ICOCEE-Cappadocia 2015- International Conference on Civil and Environmental Engineering,* May 20-23, Cappadocia, Turkey.